

Effects of Dryland Irrigation on Regional Climate
and
Air Quality in Northwest China: A Modeling Study

TAM, Hiu Fai

A Thesis Submitted in Partial Fulfilment
of the Requirements for the Degree of
Master of Philosophy
in
Earth and Atmospheric Sciences

The Chinese University of Hong Kong
July 2021

Thesis Assessment Committee

Professor LIU Lin (Chair)

Professor TAI Pui Kuen Amos (Thesis Supervisor)

Professor TAM Chi Yung Francis (Thesis Co-supervisor)

Professor LAU Ngar Cheung Gabriel (Committee Member)

Abstract of thesis entitled:

Effects of Dryland Irrigation on Regional Climate and Air Quality in Northwest China: A Modeling Study

Submitted by TAM Hiu Fai

for the degree of Master of Philosophy in Earth and Atmospheric Sciences

at The Chinese University of Hong Kong in July 2021

Abstract

Irrigation modifies regional climate and air quality by altering surface characteristics including moisture and heat fluxes. Investigating the modification of regional climate and air quality by irrigation is particularly important for semiarid regions such as Northwest China, where water resources are limited. Such modification can be substantial when compared with the relatively dry climatic background. However, how regional climate and air quality might respond to different irrigation methods remains unclear. Agricultural approaches including the deployment of different irrigation systems can be advised by optimization of water use, which is to strike a balance between irrigation, water availability, crop yields, regional climate and air quality. In this study, we studied the sensitivity of regional weather and air quality to irrigation method, a state-of-the-art climate-chemistry-land model system namely the Weather Research and Forecast Model (WRF) coupled with the GEOS-Chem (GC) chemical transport model, referred to WRF-GC, with various options to represent land surface and agricultural processes. With its ability to simulate how weather and air pollutants evolve with time, we studied the effects of implementing the “flooded”, “sprinkler”, and “drip irrigation” irrigation schemes on regional climate and air quality. The choice of soil map, soil moisture spin-up, and chemical initial and boundary conditions are

explored to improve land parameters and chemical species estimation before conducting model simulation. We found that flooded and sprinkler irrigation practices greatly reduce the sensible heat flux and increase the latent heat flux. Flooded irrigation can induce cooling of the surface up to 2°C as inferred from the averaged drop in near surface air temperature. Consequently, planetary boundary layer height decreases, which inhibits vertical mixing of air pollutants and deteriorates surface air quality. In particular, surface NO_x concentration increases by ~0.6 ppb (12%) if flooded irrigation is adopted near Xi'an of Shaanxi province. On the contrary, air quality worsening is minimized if drip irrigation is adopted, which is attributable to the minimal changes in regional climate. We conclude that drip irrigation is likely the most preferable option for semiarid agriculture, not only because of its water-saving potential but also its minimal impacts on the atmospheric environment.

摘要

透過改變地表特徵例如水分和熱通量，灌溉能夠改變區域氣候和空氣質素。因為中國西北部等半乾旱地區的水資源匱乏，所以研究灌溉對該區的天氣及空氣質素的影響尤其重要。對比其氣候相對乾燥的背景，此等改變可以很巨大。不過，我們至今未完全清楚區域氣候和空氣質素會如何因不同灌溉系統而改變。有見及此，我們希望透過找出最佳的灌溉用水模式以在灌溉、可用水、農作物產量、區域天氣及空氣質素之間取得平衡，為灌溉以至農業的未來發展提供洞見。在此研究，我們循數值模擬的方向出發，利用頂尖的天氣、化學、陸地模型，名為 WRF-GC，將天氣研究及預測模型(WRF)及 GEOS-Chem 耦合，並有不同選項用作表達地表及農作物過程。藉著其模擬未來的天氣及空氣污染物濃度的能力，我們研究了不同灌溉方式例如漫灌、噴灌、滴灌的影響。我們亦探索了土壤分佈、土壤水分、化學的初始及邊界條件以改善初始地表變數及化合物的估算。研究發現漫灌、噴灌令感熱通量大幅下降，相反潛熱通量則有所上升。對比近地面氣溫的變化，漫灌誘使的地表溫度降溫高達 2 摄氏度。結果令邊界層高度下降，抑制空氣污染物的垂直混合，使地表空氣質素轉差。假如在陝西省西安市附近實行漫灌，表面的氮氧化物上升大約 0.6ppb (12%)。相反而言，假如我們實行滴灌，能將對空氣質素的負面影響減至最低，這和滴灌對區域天氣的影響最少有關。綜上所述，滴灌擁有最大的節水潛力以及對該區環境最小的影響，所以應為最合適的灌溉選擇。

Acknowledgements

I would like to express my heartfelt thanks to my thesis supervisors Prof. Amos Tai and Prof. Francis Tam. They brought me to this exciting study which has certainly broadened my horizon and deepened my interest in weather and air quality modeling. Their valuable comments and guidance on my progress are crucial to make this study meaningful and impactful, and more importantly, such guidance is inspiring that is useful to my future career and many other relevant tasks.

It is my great pleasure to join Prof. Amos Tai's and Prof. Francis Tam's research groups at the same time. It is worth appreciating as this has given me a comprehensive overview of slightly different kind of atmospheric modelers.

I wish to thank my thesis assessment committee including Prof. Liu and Prof. Gabriel Lau for their constructive comments that greatly improved this study.

My sincere gratitude also goes to my family, my girlfriend Florence Lapto, and my friends. I spent much more time at home during the special work from home arrangement due to the pandemic and my family and girlfriend provide great care and room. Although my girlfriend's research focuses on criminology, her research insights can also be applied to my field of study and further polish my way of thinking and writing. I also wish to express my heartfelt thanks to her love and care. My friends also relieve my pressure a lot during this special and fast-changing environment.

Table of Contents

Abstract.....	i
Acknowledgements.....	iv
List of Figures	vii
List of Tables	xi
1. Introduction	1
2. Data and methods.....	8
2.1 Model description.....	8
2.2 Irrigation parameterization.....	10
2.3 Model initialization.....	13
2.3.1 Soil map.....	15
2.3.2 Model spin-up	19
2.3.3 Chemistry input.....	22
2.4 Crop distribution	26
2.5 Site-level irrigation and its impacts to the surface	27
3. Results and discussion.....	32
3.1 Hypothetical experiments.....	32
3.2 Production simulations	34
3.2.1 Regional weather modification	34
3.2.2 Regional air quality modification.....	41
3.3 Vertical structure.....	44
3.4 Site-level time series comparison.....	46
4. Conclusions and future work	50
Appendices	52
Appendix A. Simulation of the inner domain	52

Appendix B. Irrigation parameterization based on realistic irrigation amount..	58
Bibliography	61

List of Figures

Figure 1. Coverage of the domain. It covers Northwest China such as the Gansu, Shaanxi, Hubei provinces.....	9
Figure 2. (Left) Area equipped for irrigation and (right) area actually irrigated divided by area equipped for irrigation from the AQUASTAT database, the Food and Agriculture Organization of the United Nations (FAO).....	10
Figure 3. (Left) Weather observation sites and (bottom) air quality measurement sites in the domain.....	15
Figure 4. (Left) WRF default soil map and (right) Beijing Normal University (BNU) soil map of the domain. There are substantial differences in the soil type. For example, soil in some parts of Sichuan and Shanxi provinces changes from clay loam to loam.....	16
Figure 5. Change in 2-m temperature when the simulation changes from WRF default soil to Beijing Normal University (BNU) soil map. The differences are correlated with the change in the soil type, which affects the land-atmosphere interactions by changing the prescribed soil parameters such as saturated and wilting point soil moisture.....	17
Figure 6. Scatter plots of simulated 2-m temperature against observed temperature of (top) default soil and (bottom) Beijing Normal University (BNU) soil. Verification indicates that using BNU soil does not improve the simulation as depicted by the very similar slope and y -intercept of the linear fitting line. Nevertheless, the BNU soil map was adopted in this study because the resolution is higher and the dataset is based on more recent observations specifically in China.	19
Figure 7. Time series of surface soil moisture during the two-year simulation of (orange) without fixing atmospheric forcing and (blue) with fixing atmospheric	

forcing. The two lines overlap each other in the first year because they are identical in both model and initial, boundary conditions.....	20
Figure 8. Soil moisture distribution on 1 July 2017 in the Northwest China domain in (top) spin-up case; (middle) right at model initialization without any spin-up; (bottom) GLEAM version 3.5a.....	21
Figure 9. Scatter plot of (top) MOZART-4 and (bottom) GEOS-Chem (GC) simulated against observed ozone concentration averaged daily by observation sites. GC reduces the high-biases in ozone simulations compared with MOZART-4.	24
Figure 10. Scatter plot of (top) MOZART-4 and (bottom) GEOS-Chem (GC) simulated against observed NO ₂ concentration averaged daily by observation sites. The performances of MOZART-4 and GC are comparable.	25
Figure 11. Most common crops present in our Northwest China domain as depicted by the crop functional type of Community Land Model version 5.0 (CLM5).	26
Figure 12. Time series of surface soil moisture from (blue) farm with flooded irrigation and (red) farm with drip irrigation. Irrigation is deployed when the surface soil moisture drops to a certain threshold.	28
Figure 13. Time series of surface soil temperature from (blue) farm with flooded irrigation and (red) farm with drip irrigation. In general, the soil temperature is lower over the farm with flooded irrigation.	29
Figure 14. Time series of (top) latent heat flux and (bottom) sensible heat flux from (blue) farm with flooded irrigation and (red) farm with drip irrigation. Latent heat flux (sensible heat flux) is higher (lower) in the flooded case compared with the drip case.....	30
Figure 15. Soil moisture at the time three days after the initial condition of control run, hypothetical flooded irrigation, sprinkler irrigation, and drip irrigation. The	

arrows represent 10-m wind field.....	32
Figure 16. 2-m air temperature at the time three days after the initial condition of control run, hypothetical flooded irrigation, sprinkler irrigation, and drip irrigation.	
The arrows represent 10-m wind field.	33
Figure 17. Cloud fraction at the time three days after the initial condition of control run, hypothetical flooded irrigation, sprinkler irrigation, and drip irrigation. The arrows represent 10-m wind field.....	34
Figure 18. Soil moisture difference of flooded irrigation compared with control run. The increase in soil moisture represents the regions that are irrigated according to FAO irrigation mask and the irrigation threshold. Some regions equipped with irrigation are not irrigated in the model because the soil moisture does not fall below the irrigation threshold.	35
Figure 19. 2-m air temperature difference of flooded irrigation, sprinkler irrigation, and drip irrigation compared with the control run (without irrigation).....	37
Figure 20. Latent heat flux difference of flooded irrigation, sprinkler irrigation, and drip irrigation compared with the control run.	38
Figure 21. Sensible heat flux difference of flooded irrigation, sprinkler irrigation, and drip irrigation compared with the control run.	39
Figure 22. Changes in surface pressure, wind field, 10-m <i>u</i> -wind component, and 10-m <i>v</i> -wind component of the flooded irrigation case compared with the control run. 41	
Figure 23. Scatter plot of (left) control and (right) flooded irrigation simulation against observation.....	41
Figure 24. Change in NO _x concentration of flooded irrigation, sprinkler irrigation, and drip irrigation compared with control run.	42
Figure 25. Change in ozone concentration of flooded irrigation, sprinkler irrigation,	

and drip irrigation compared with control run.....	43
Figure 26. Vertical profiles of (left) mixing ratio, (right) potential temperature as simulated for irrigated grid cells near Xi'an of Shaanxi province over daytime.....	45
Figure 27. Vertical profiles of (left) NO _x , (right) CO as simulated for some irrigated grid cells near Xi'an of Shaanxi province over daytime.....	45
Figure 28. Vertical profile of ozone as simulated for some irrigated grid cells near Xi'an of Shaanxi province over daytime.....	46
Figure 29. 2-m air temperature time series of observation and simulations at a weather station located near Xi'an, Shaanxi province (34.4N, 108.8E). Simulation of flooded irrigation matches with observations better than the others.....	48
Figure 30. Time series of observed and simulated ozone (daily maximum 8-hourly average, DMA8), NO ₂ , and CO in a air quality observation site near Xi'an. Compared with the simulated 2-m air temperature, our simulations cannot capture the actual value of species concentrations well yet the trend is in fair agreement for NO ₂	49
Figure A1. Coverage of the inner domain.....	54
Figure A2. Time series of site observation, and corresponding WRF-GC simulations of (top) 2-m air temperature, (middle) sensible heat flux, (bottom) latent heat flux using Noah and Noah-MP as the LSMs.....	55
Figure A3. Modified initial temperature field of the inner domain using OBSGRID.....	56
Figure A4. (Top) initial field after nudging all WMO observations; (bottom) temperature difference field after 3 hours of simulation. It can be seen that even with observations nudged, the model is likely to return to its original state after a few hours.....	57

Figure B1. The temperature difference of option 1, option 2, option 3 compared with the control run that does not incorporate any irrigation in the same model..... 59

List of Tables

Table 1. Physics and chemical parameterization schemes used.	8
Table 2. Proportion of different irrigation systems implemented in China, 2006 from FAO.	11
Table 3. Details of initialization experiments of varying chemical initial and boundary conditions, choice of soil map, and whether we adopt a spin-up for the soil moisture.	14
Table 4. Soil parameters in Noah-MP. The unit of wilting point, field capacity, saturation soil moisture is m ³ /m ³	16

1. Introduction

Agricultural irrigation is a substantial consumer of water that accounts for 70% of all freshwater withdrawals (Food and Agriculture Organization of the United Nations (FAO), 2007). In 2017, China agricultural water withdrawal was 385.2 billion per year, which was 64% of the total water withdrawal (FAO, 2021). Irrigation water is applied mainly through surface irrigation methods, accounting for 94.0% of the total irrigation amount; localized irrigation, which is a more advanced irrigation technique, consisted of 1.2% only (FAO, 2021). Effective irrigation is important to secure food production as Northwest China suffers from serious water shortage (Kang et al., 2017). Climatologically, Northwest China has a dry climate because it is located at the innermost center of the Eurasian continent and its long distance to the oceans (Shi et al., 2007) such that water resources for irrigation are scarce (Shen et al., 2013). Implementation of more advanced irrigation technologies is under active research to optimize water use efficiency and crop yield in terms of soil water (Yang et al., 2017) and nutrient management (Zhang et al., 2009). For instance, drip irrigation is a kind of advanced irrigation technology that saves water, allows fertilization, improves crop yield, reduces evaporation and soil degradation (Liu et al., 2012). There are farms with drip irrigation implemented for different crops in Northwest China, including potato (Hou et al., 2010; Zhang et al., 2017), cotton (Kang et al., 2012; Wang et al., 2014), maize (Zou et al., 2020), grapes (Li et al., 2020), etc. Maize is one of the major cereal crops in the semiarid region of Northwest China and it contributes 53.1% to China total food production (Zou et al., 2020). Wang et al. (2020) conducted experiment using two mulched maize fields, one with border irrigation and the other with drip irrigation. The daily evaporation rate decreased by 0.13 mm per day whereas daily

transpiration rate increased by 0.19 mm per day. In these studies, drip irrigation promoted crop yield by reducing evaporation, increasing soil temperature, and lengthening the growing season. These studies are important to address the issue of which irrigation system to be implemented in the local perspective in order to improve water-saving and crop yield, but they are also crucial to simulate such effects in a regional manner particularly the modifications to weather and air quality that in turn affect crop yield. Currently a complete understanding on how to strike a balance between optimizing water usage through different irrigation techniques, impacts on regional weather and air quality is lacking.

Heihe river basin is an important surface water source where 84% of the total water source is consumed by agricultural irrigation (Ge et al., 2013). Mean annual precipitation is 120 mm whereas mean annual potential evaporation is approximately 1410 mm due to abundant sunshine. There is a deficit in irrigation water source thus improving agricultural water management is in great demand. From the data of China Irrigation and Drainage Development Center, the daily irrigation water applied over the whole China is 2.96 mm. In Northwest China where a typical growing season lasts for 5 months, the total irrigation water consumed in a growing season is about 444 mm. This is consistent with field data recorded at two maize farms in Gansu province (Wang et al., 2020), in which the 2017 growing season consumed about 600 mm irrigation water with border irrigation deployed, whereas another maize farm equipped with drip irrigation consumed about 320 mm irrigation water, which demonstrated substantial water saving potential. Although drip irrigation greatly reduces the demand of irrigation water, there is still a deficit in water because evaporation largely exceeds precipitation over the region. As a consequence, groundwater is also being exploited to fulfill the irrigation demand.

Fundamentally, irrigation adds water onto either land surface or soil regardless

of which irrigation system being used. Irrigation reshapes regional weather and air quality by modifying surface characteristics such as albedo, heat capacity, near-surface temperature and moisture gradients that would affect surface energy balance and partitioning. Surface sensible heat flux (H) measures the conductive heat flux from the surface to the atmosphere while latent heat flux (λE) measures a similar energy flux but related to evaporation or transpiration of water at the surface. They are mathematically related to the respective gradients through the following equations:

$$H = -\rho c_p K_h \frac{\partial T}{\partial z} \quad (1)$$

$$\lambda E = -\rho K_w \frac{\partial q}{\partial z} \quad (2)$$

where ρ is the mass density of air, c_p is the specific heat capacity of air, K_h and K_w are the eddy diffusivities for heat and water vapor respectively, T is the temperature, and q is the specific humidity. As land surface moisture increases, the moisture gradient from surface to atmosphere increases. It can be seen from equation (2) that latent heat flux increases with increasing moisture gradient. At the same time, the irrigation water added to the surface increases the heat capacity of the surface, which diminishes diurnal variations of near-surface temperature. Reduced near-surface temperature during daytime reduces temperature gradient from surface to the atmosphere. As a result, surface sensible heat flux decreases whereas latent heat flux increases if irrigation is applied. This result also matches with theoretical understanding in the surface energy balance perspective with the following equation:

$$R_n = H + \lambda E + G \quad (3)$$

where R_n is the net radiation absorbed, H is the sensible heat flux, λE is the latent heat flux, and G is the ground heat flux. Assuming albedo to be a constant, R_n can also be taken as a constant and the three fluxes on the right hand side of equation (3) balance each other. The surface energy balance equation thus suggests an increase in H would

be balanced by a decrease in λE and vice versa.

Reduced sensible heat flux improves atmospheric stability as less energy transferred to the atmosphere would lead to a less convective atmosphere. Atmospheric stability can be characterized by the potential temperature gradient. Potential temperature (θ) is the temperature that an air parcel would attain if it is brought adiabatically to the reference pressure level (1000 hPa). The atmosphere is stable if any displaced parcel would restore its original position due to the buoyant force that emerges from the density difference between the parcel and the environment. Since density and temperature are related, it can be transformed to the potential temperature gradient mathematically. As potential temperature usually increases with height in light of the atmosphere is generally stable, the induced cooling in near-surface potential temperature by irrigation would lead to an increase in potential temperature gradient, further improving the stability of the atmosphere.

$$\begin{cases} \frac{\partial \theta}{\partial z} > 0 & (\text{stable}) \\ \frac{\partial \theta}{\partial z} = 0 & (\text{neutral}) \\ \frac{\partial \theta}{\partial z} < 0 & (\text{unstable}) \end{cases}$$

Vertical mixing of air parcels would then be inhibited that can cause substantial impact to surface air quality. Air pollutants are mostly emitted near-surface. Human activities such as emissions from power plants, motor vehicles, industrial activities release air pollutants including NO_x , SO_2 , CO . In particular, part of Gobi Desert is located in Northwest China, which is a dust source such that particulate matter (PM) can be advected to provinces with denser population under suitable wind direction and atmospheric stability. Taking all these emitted species and the improved atmospheric stability into consideration, it can be anticipated that surface air quality would generally worsen after applying irrigation, which is an adverse impact that we want to

avoid by selecting a better irrigation system and strategy.

Regional weather and air quality modification due to irrigation has been more widely studied in the Central Valley of California, USA, which is one of the most productive agricultural regions in the world. Li et al. (2016) used Weather Research and Forecast Model with Chemistry (WRF-Chem) to perform simulations of irrigation methods implemented in the model to study the effects on weather and air quality in the Central Valley. They found that with irrigation implemented, primary pollutant concentrations (e.g. CO, NO_x, VOC) increases, but surface ozone concentration decreases in the irrigated region. The modified regional weather drives the ozone precursors away from the irrigated region, causing ozone to form in the surroundings of the valley. The worsened air quality overall can be attributed to the decreased turbulence and instability, weakening vertical mixing. Lawston et al. (2015) studied the effects of different irrigation schemes using WRF over the central Great Plains of the US. The findings on weather changes are similar to that of Li et al. (2016), emphasizing that weather changes can be advected to the surroundings of the densely irrigated area and cause weather modification on a larger regional scale.

There are also several studies that investigated irrigation in Northwest China. Zhang et al. (2017) implemented an irrigation scheme that adds water if there is a soil moisture deficit using WRF and Noah-MP (Niu et al., 2011). In the irrigated simulation, there is a large increase in latent heat and decrease in sensible heat, leading to more humid and cooler surface air. The effects are diminished at approximately 600 hPa. The pattern of change in precipitation appears mixed, with decreased precipitation over the irrigated field because of higher stability, but some parts of the domain receives more precipitation because of intensified water vapor fluxes. Another study by Wu et al. (2020) also focused on Northwest China and implemented mulching into the

irrigation scheme. The plastic film mulch helps keep energy and moisture near the surface, thus reducing latent heat flux and enhancing sensible heat flux. Rising surface temperature also lengthens the growing season. The prevention of evapotranspiration from the soil and crops to the atmosphere reduces the amount of water vapor in the atmosphere and thus decreases precipitation.

In addition to regional weather and air quality modification, the relationship between irrigation, global climate, and some extreme weather events (e.g. heatwave, drought) also gained researchers' interest. Sacks et al. (2009) examined how irrigation would affect climate over the globe by running CAM coupled with CLM for 30 years. Intuitively irrigation cools the surface by adding more water that enhances evaporative cooling, there are regions where near-surface temperature increases due to modified circulation patterns. The effects are comparable to that of changing land surface type that causes temperature change of about 1°C. Clouds also play an important role to cool the surface on top of radiative cooling. Overall in the global perspective, irrigation induced cooling are balanced by an increase in temperature over some particular regions because circulation patterns are modified such that global surface temperature only changes by a little amount on average.

Valmassoi et al. (2020) used WRF to study the impacts of irrigation on regional climate during heatwave in Po Valley of Northern Italy. It is found that irrigation can mitigate the intensity of heatwave by lowering surface temperature. As the irrigation water increases soil moisture and thus modifies surface energy fluxes, surface temperature decreases up to 2.5 - 3°C during the month affected by heatwave, and up to 0.75 - 1°C for another month without heatwave. However, the synoptic patterns that caused the heatwave to occur remain unaffected in this particular case. In general, the modification of regional climate (e.g. precipitation, temperature, moisture) affects heatwave formation because evapotranspiration, soil moisture, etc. changes such that

the intensity of heatwave is also reduced. It is important to emphasize that heat stress and heat discomfort may not decrease due to the increase in surface moisture that prohibits evaporative cooling particularly overnight. Mishra et al. (2020) also used WRF to study irrigation and heat stress over India. They found that moist heat stress increases and affects 37 - 46 million people despite land surface and the air cools by 1°C and 0.5°C respectively.

Ambika et al. (2020) studied the ease of drought over India due to irrigation using WRF. After implementing irrigation, atmospheric aridity decreases yet soil moisture and relative humidity increases. It also has a substantial role in greening by increasing leaf area index (LAI), gross primary production (GPP) and net primary production (NPP). These effects together with the modified surface energy balance moderate the risk of drought, with temperature decreases by about 0.8 °C and relative humidity increases by about 2%.

With an aim to optimize irrigation water usage over semiarid regions such as Northwest China, this study used WRF-GC (WRF coupled with the GEOS-Chem chemical transport model) to simulate how regional weather and air quality respond to different types of irrigation. It is an online model coupling land surface model (LSM), weather model (WRF) and chemical transport model (GEOS-Chem). The irrigation schemes follow those by Lawston et al. (2015), with additional analysis of air quality because WRF-GC is capable of simulating emissions, atmospheric chemistry, transport and deposition of different chemical species following WRF atmospheric dynamics. The simulated results would be useful to quantify the impacts of different irrigation systems to regional climate and air quality, which serves as references for policy makers and farmers to determine the most preferred irrigation system for the region to optimize water-saving, crop yield, and potential health impacts.

2. Data and methods

2.1 Model description

The WRF-GC model (Weather Research and Forecast model coupled with GEOS-Chem) version 1.0 (Lin et al., 2020) was used to conduct regional weather and air quality simulations. It consists of dynamic core WRF model version 3.9.1.1 and the GC version is 12.2.1. In WRF-GC version 1.0, there is only one-way coupling, meaning that atmospheric chemistry is affected by meteorology but not the other way round. The two-way coupling is available in WRF-GC version 2.0 (Feng et al., 2021) but the effects of the two-way processes available (e.g., aerosol-radiation interactions) are expected to be negligible in this study. Table 1 shows the details of the physics and chemical parameterization schemes adopted in our model setting.

Table 1. Physics and chemical parameterization schemes used.

Land Surface Model (LSM)	Noah (Chen et al, 2001), Noah-MP (Niu et al., 2011)
Cumulus Parameterization	New-Tiedtke Scheme (Zhang et al., 2017)
Microphysics	Morrison Double-Monment Scheme (Morrison et al., 2009)
Boundary Layer	YSU Scheme (Hong et al., 2006)
Long-wave, Short-wave Radiation	RRTMG (Mlawer et al, 1997)
Convection, Emission, PBL Mixing, Chemistry,	GEOS-Chem (HEMCO responsible for emission)
Dry deposition, Wet deposition	

The area of this study focused on Northwest China, where mountain ranges are found in the western side over Qinghai province and Tibet, and low-lying areas with agricultural activities are found in the eastern side such as over Shanxi and Hubei provinces. Gansu province is adjacent to the high grounds with relatively dry climatic background that mainly produces maize and wheat. Figure 1 shows the domain of the simulation in $9\text{ km} \times 9\text{ km}$ resolution covering Northwest China. The meteorological initial and boundary conditions were from National Centers for Environmental Prediction (NCEP) Final (FNL) Operational Global Analysis data with $1^\circ \times 1^\circ$ spatial resolution, and the temporal resolution is 6-hour. The number of grid cells was 245 by 181. The vertical coordinate used was the hybrid sigma-eta coordinate with 50 vertical levels. The chemical initial and boundary conditions were from either MOZART-4 (Emmons et al., 2010) or GC. The spatial resolutions of MOZART-4 and GC are $1.9^\circ \times 2.5^\circ$ and $2^\circ \times 2.5^\circ$ respectively.

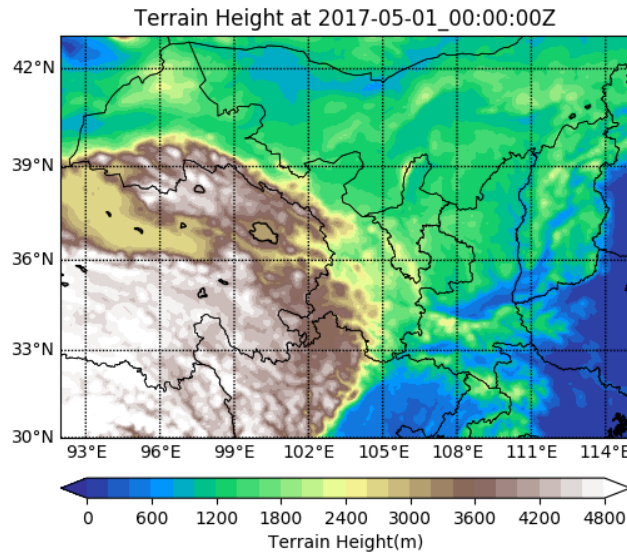


Figure 1. Coverage of the domain. It covers Northwest China such as the Gansu, Shaanxi, Hubei provinces.

2.2 Irrigation parameterization

Following Lawston et al. (2015), three different types of irrigation, namely flooded irrigation, sprinkler irrigation and drip irrigation were implemented into the land surface model Noah-MP (Niu et al., 2011). Noah-MP has better soil representation than Noah such as improved subsurface runoff and infiltration, single-layer canopy, multi-layer snow, etc. In general, Noah-MP also improves fluxes estimates compared with the original Noah land surface scheme. To minimize water loss, irrigation was implemented to start in the small hours (2 am local time) such that evaporation is minimum. The irrigated cells made reference to the AQUASTAT database of the FAO following the codes developed by Valmassoi et al. (2020). Figure 2 shows the irrigated cell in our domain using the AQUASTAT database. The proportion of the area actually irrigated over the area equipped for irrigation is very high as seen in Figure 2, thus we used the area equipped for irrigation to irrigate our model without any weighting. Table 2 shows the details of irrigation systems that were in use over China in 2006. Surface irrigation was the most dominant irrigation type that accounts for 94.0%.

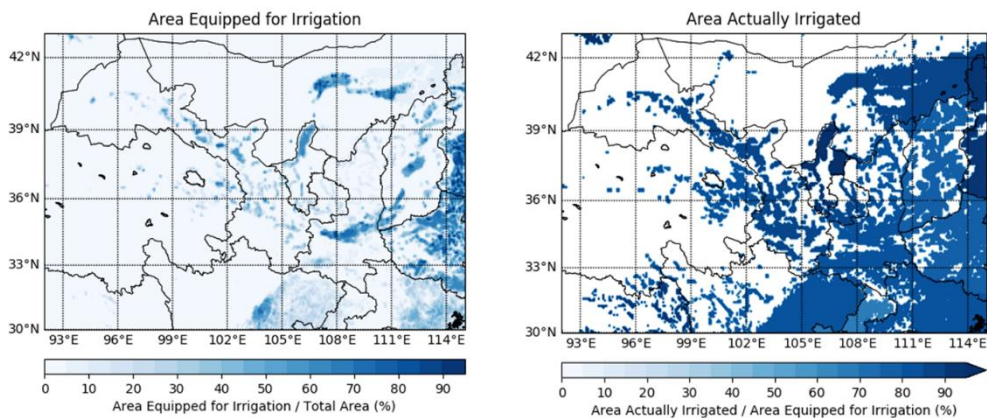


Figure 2. (Left) Area equipped for irrigation and (right) area actually irrigated divided by area equipped for irrigation from the AQUASTAT database, the Food and

Agriculture Organization of the United Nations (FAO).

Table 2. Proportion of different irrigation systems implemented in China, 2006 from FAO.

Irrigation type	Area equipped in China (1000 ha)
Surface Irrigation (Furrow, Flooded)	59338 (94.0%)
Sprinkler Irrigation	2841 (4.5%)
Localized Irrigation (Drip)	759.5 (1.2%)
Total	62938 (100%)

Flooded irrigation is a traditional and low-cost way of surface irrigation; it lets water flow down trenches in the periphery of the crops. Due to the abundant amount of irrigation water added and infiltrating into the soil, there is less evaporation compared with other irrigation practices; however, water loss near the edges through runoff can be prominent. Evans and Zaitchik (2008) simulated flooded irrigation by applying irrigation water to saturate the topsoil layer in view of the abundance of water infiltrated into the soil, and flooded irrigation is parameterized as fixing soil moisture (SMC) into its field capacity at the irrigation time, which is also in good agreement with field data.

Sprinkler irrigation is an analog to household gardening that sprays water onto the surface through tiny water droplets. Ozdogan et al. (2010) demonstrated irrigation simulation in the form of adding precipitation by considering root-zone moisture availability. It is not widely adopted in Northwest China and requires substantial amount of machinery. Nonetheless, water loss using sprinkler irrigation is theoretically higher than flooded irrigation since more water is sprayed onto the surface and evaporate, subject to surface weather conditions. In LSM, it is

represented by adding additional rainfall of 5 mm/h; otherwise there is no change in the model.

In general, it is agreed that irrigation parameterizations can be represented by different variables in WRF, including soil moisture, precipitation, evapotranspiration etc. However, there are inconsistencies in quantifying the irrigation threshold and the amount of irrigation water being used in the model (Leng et al., 2017). Flooded irrigation is usually mimicked by adding soil moisture directly. There are studies that bring the top layer of soil to saturation to mimic flooded irrigation (Evans and Zaitchik, 2008; Lawston et al., 2015; Yilmaz et al., 2014; Zaitchik et al., 2005). There are other studies that raise soil moisture to the field capacity instead (Huber et al., 2014; Kueppers et al., 2007; Sorooshian et al., 2011). A complete justification on the soil moisture being added is lacking.

Similarly for sprinkler irrigation, although it is widely mimicked by adding precipitation, the amount of irrigation water varies. Pei et al. (2016) implemented a precipitation rate of 20 mm per hour based on estimation of pumping water supply and discussing with farmers. Yang et al. (2019) took a step further to estimate the irrigation water amount by comparing the current moisture content with the field capacity. There are also studies that implicitly add water in the form of precipitation (e.g. Wu et al., 2020). Nonetheless, it is emphasized that the amount of irrigation water in any irrigation parameterization represents a mixture of crop and soil in the coarse grid box. The actual amount of irrigation water may thus differ from the prescribed value in the model.

It is suggested that the timing of irrigation within a day is important in order to minimize evaporation. Valmassoi et al. (2020) studied the sensitivity of irrigation timing to the impacts of irrigation. There is no significant impact of the irrigation timing to effects that are beyond diurnal cycle such as modification of fluxes, soil

moisture. The irrigation timing only affects these variables within the diurnal cycle.

Drip irrigation is a more modernized irrigation scheme with pipe network installed in the farming site. Water is supplied through the dense pipes directly onto the crops. The irrigation time and amount of water can be easily controlled through centralized computer system. Using such architecture, we assume that the crops would not experience water stress and the amount of water is just right enough for crops to transpire. In the model, transpiration is tuned up to the maximum value when it is irrigation time. Although water is not directly added in the LSM to mimic irrigation, the resultant weather and air quality would still be affected because of changes in canopy resistance (Evans and Zaitchik, 2008) and thus biosphere-atmosphere fluxes.

2.3 Model initialization

There are three aspects in model initialization of different model components, including soil distribution, soil moisture spin-up, and chemical initial and boundary conditions. The default soil distribution used in WRF is from the US Geological Survey (USGS). It is dated compared with the simulation that we are interested in, as it was created based on radiometer scanning from April 1992 to March 1993 (Dy and Fung, 2016). A more recent soil distribution dataset was generated by Beijing Normal University (BNU) in 2013 that provides higher resolution soil data for WRF. In addition, the BNU dataset is based on databases and measurements in China. Little attention has been paid to fine tune the variables related to soil in WRF (e.g., soil temperature and moisture) due to lack of extensive in-situ observations. The simulated soil moisture drifted away from its initialized value and took 2 to 3 years to stabilize (Dy and Fung, 2016). It is suggested that proper spinning-up of soil moisture can improve land-atmosphere interactions and reduce temperature biases. For chemistry inputs, the species concentrations can be provided by any chemical

transport model, and in this study two common input data source including MOZART-4 and GC were examined. With the above initializations, four model experiments were conducted with details listed in Table 3.

Table 3. Details of initialization experiments of varying chemical initial and boundary conditions, choice of soil map, and whether we adopt a spin-up for the soil moisture.

Simulation	Chemical Initial & Boundary Conditions	Soil Map	Soil Moisture Spin-up
Simulation 1	MOZART	Default	None
Simulation 2	GC	Default	None
Simulation 3	MOZART	BNU	None
Simulation 4	MOZART	Default	2-year spin-up

The simulations were verified in both meteorological and chemical aspects. Meteorologically, the weather observations were taken from weather stations that are recognized by the World Meteorological Organization (WMO). The National Climatic Data Center (NCDC) stores these observations and provides hourly observations of temperature, dew point, wind speed, and wind direction. Observations are evenly distributed in the domain. For verifying the species concentrations, observational data was taken from stations managed by China National Environmental Monitoring Centre (CNEMC), with species including PM_{2.5}, PM₁₀, ozone, NO₂, and SO₂. The distribution of the air quality stations is different from that of the weather observation since air quality stations are mostly deployed in the vicinity of densely populated cities. Figure 3 shows the distributions of the

weather observation and air quality measurement stations.

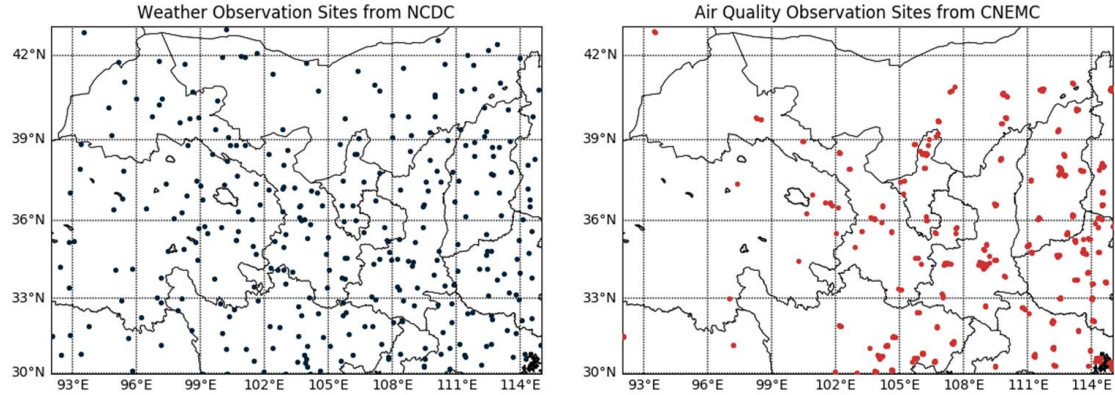


Figure 3. (Left) Weather observation sites and (bottom) air quality measurement sites in the domain.

2.3.1 Soil map

In the model, soil is important to characterize crucial variables such as heat fluxes by the spatial distribution of soil type and parameters including wilting point, field capacity, etc. Figure 4 shows the differences of the default soil map of WRF and the BNU soil map. The soil type changes from clay loam to loam in some parts of the Sichuan and Shanxi provinces. Since loam holds less water in the soil representation of the land surface model (LSM) due to lower saturated and wilting point soil moisture (see Table 4 for the soil categories and their corresponding values of parameters), such regions experience a drop in 2-m temperature because of more moisture above the surface. Figure 5 shows the corresponding change in temperature distribution.

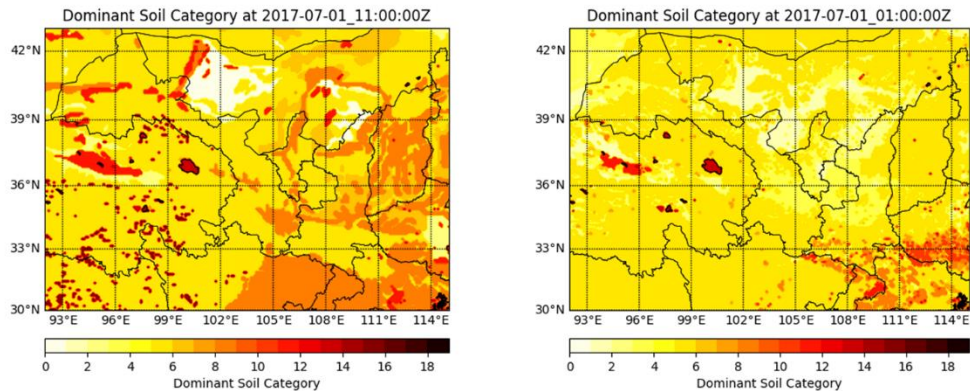


Figure 4. (Left) WRF default soil map and (right) Beijing Normal University (BNU) soil map of the domain. There are substantial differences in the soil type. For example, soil in some parts of Sichuan and Shanxi provinces changes from clay loam to loam.

Table 4. Soil parameters in Noah-MP. The unit of wilting point, field capacity, saturation soil moisture is m^3/m^3 .

ID	Name	Wilting Point	Field Capacity	Saturation soil moisture
0	Sand	0.010	0.236	0.339
1	Loamy sand	0.028	0.383	0.421
2	Sandy loam	0.047	0.383	0.476
3	Silt loam	0.084	0.360	0.476
4	Silt	0.084	0.383	0.476
5	Loam	0.066	0.329	0.439
6	Sandy clay loam	0.067	0.314	0.404
7	Silty clay loam	0.120	0.387	0.464

8	Clay loam	0.103	0.382	0.465
9	Sandy clay	0.100	0.338	0.406
10	Silty clay	0.126	0.404	0.468
11	Clay	0.138	0.412	0.468
12	Organic material	0.066	0.329	0.439
13	Water	0.000	0.000	1.000
14	Bedrock	0.006	0.170	0.200
15	Other	0.028	0.283	0.421
16	Playa	0.030	0.454	0.468
17	Lava	0.006	0.170	0.200
18	White sand	0.010	0.236	0.339

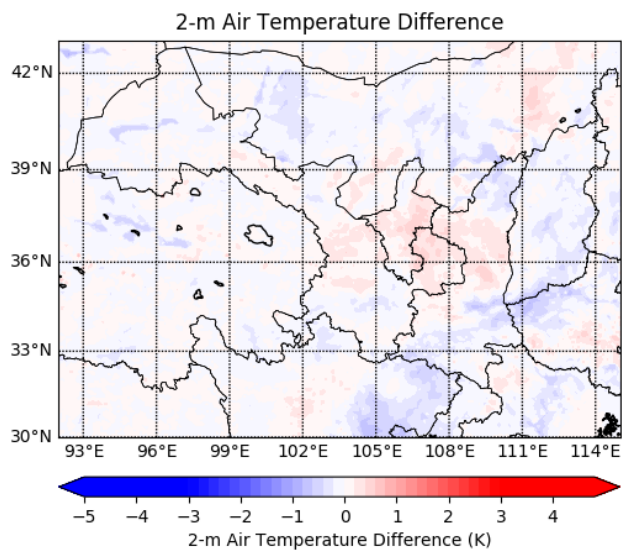
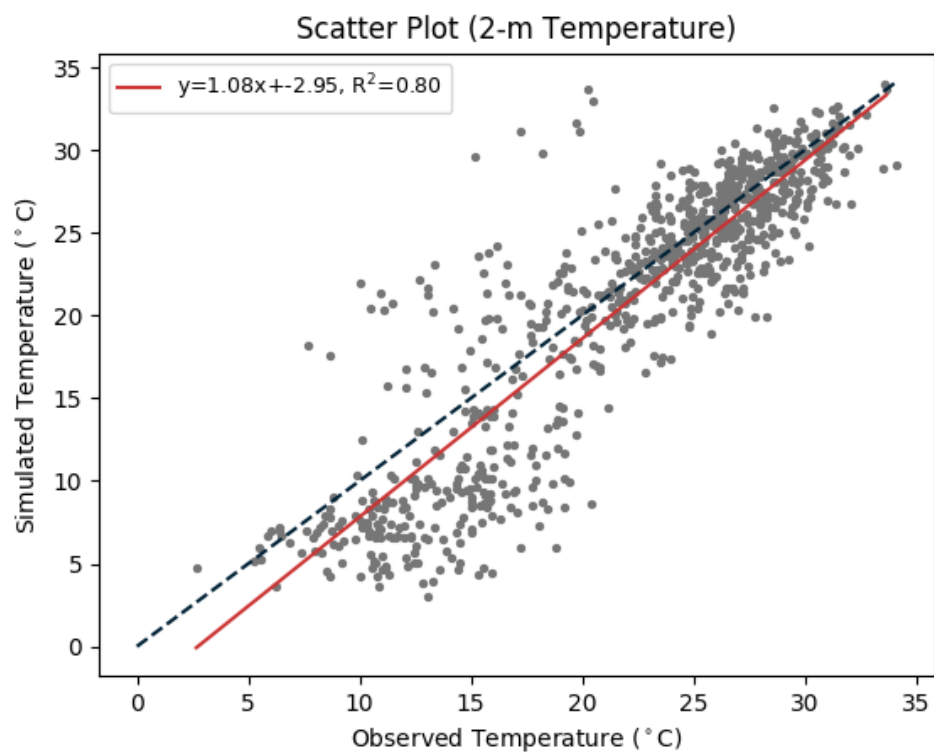


Figure 5. Change in 2-m temperature when the simulation changes from WRF default soil to Beijing Normal University (BNU) soil map. The differences are correlated with the change in the soil type, which affects the land-atmosphere interactions by changing the prescribed soil parameters such as saturated and wilting point soil moisture.

By comparing the results with observations, we found that using BNU soil does not improve the simulation in terms of reproducing the observations. Figure 6 shows the scatter plots of simulated 2-m air temperature against observed temperature. The simulated temperature was directly taken using the value from the closest grid box. The linear fits of both distributions are very similar as shown by the slope and y-intercept of the fitting line.



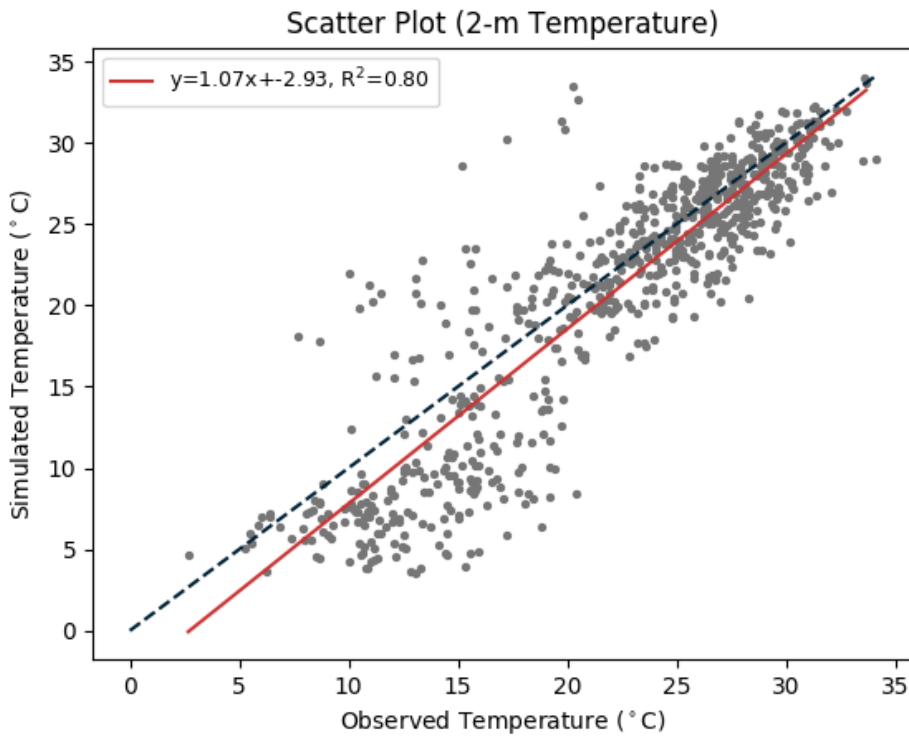


Figure 6. Scatter plots of simulated 2-m temperature against observed temperature of (top) default soil and (bottom) Beijing Normal University (BNU) soil. Verification indicates that using BNU soil does not improve the simulation as depicted by the very similar slope and y -intercept of the linear fitting line. Nevertheless, the BNU soil map was adopted in this study because the resolution is higher and the dataset is based on more recent observations specifically in China.

2.3.2 Model spin-up

Since our study focuses on land-atmosphere interactions and irrigation practices, proper spin-up of the land surface is crucial to improve the simulations. We performed two-year spin-up from July 2015 to June 2017 to investigate the variations of land parameters during these two years. In view of the Courant–Friedrichs–Lewy condition, we ran this spin-up simulation using coarser resolution of $27\text{ km} \times 27\text{ km}$ at the expense of increasing the time step from 30 seconds to 150 seconds. The domain

covers the whole China and other settings including the choice of LSM and parametrizations remain the same as other simulations. Figure 7 shows the time series of soil moisture within these two years for the whole domain.

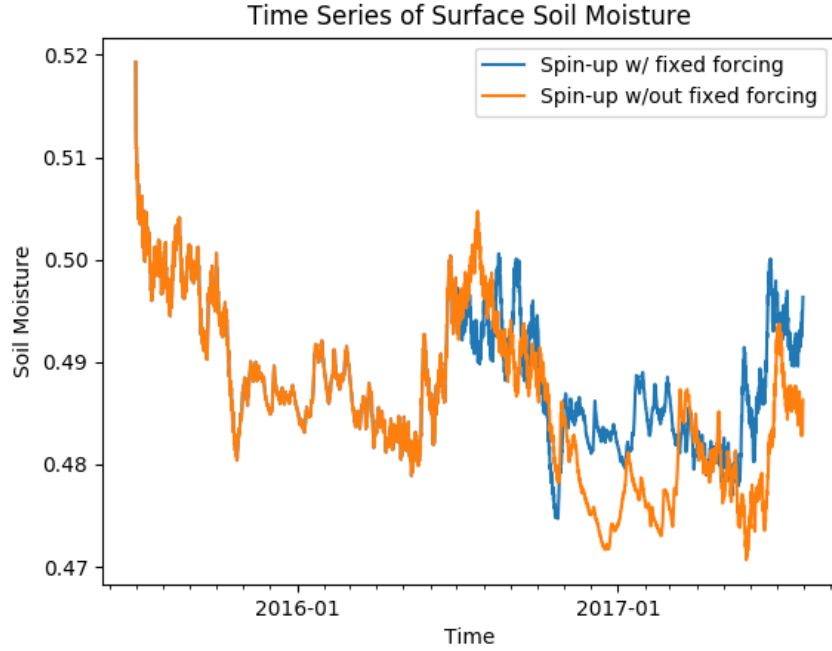


Figure 7. Time series of surface soil moisture during the two-year simulation of (orange) without fixing atmospheric forcing and (blue) with fixing atmospheric forcing. The two lines overlap each other in the first year because they are identical in both model and initial, boundary conditions.

It is found that the initial soil moisture is at its peak right at model initialization and starts to drop as time evolves. The time series demonstrates clear seasonal variation: summer (June, July, August) has the highest soil moisture whereas other months are relatively dry. To further eliminate year-to-year variability, we used the same set of meteorological input for the boundary conditions from July 2015 to June 2016 to replicate the same weather condition for the second year. In Figure 7 the blue line shows the modified time series in this setting.

After eliminating year-to-year variability, soil moisture is found to fluctuate steadily between ~ 0.48 to ~ 0.50 from dry to wet season, which is about 5% different from the initial value. In other words, using the soil moisture being spun up helps reduce error in soil moisture by about 5%, and the stabilized soil moisture field is more robust as irrigation timing, land surface parameters and processes are better represented. Figure 8 shows the soil moisture in the Northwest China domain in three different cases: (i) with spin-up; (ii) without spin-up, and (iii) Global Land Evaporation Amsterdam Model (GLEAM) dataset (Martens et al., 2017).

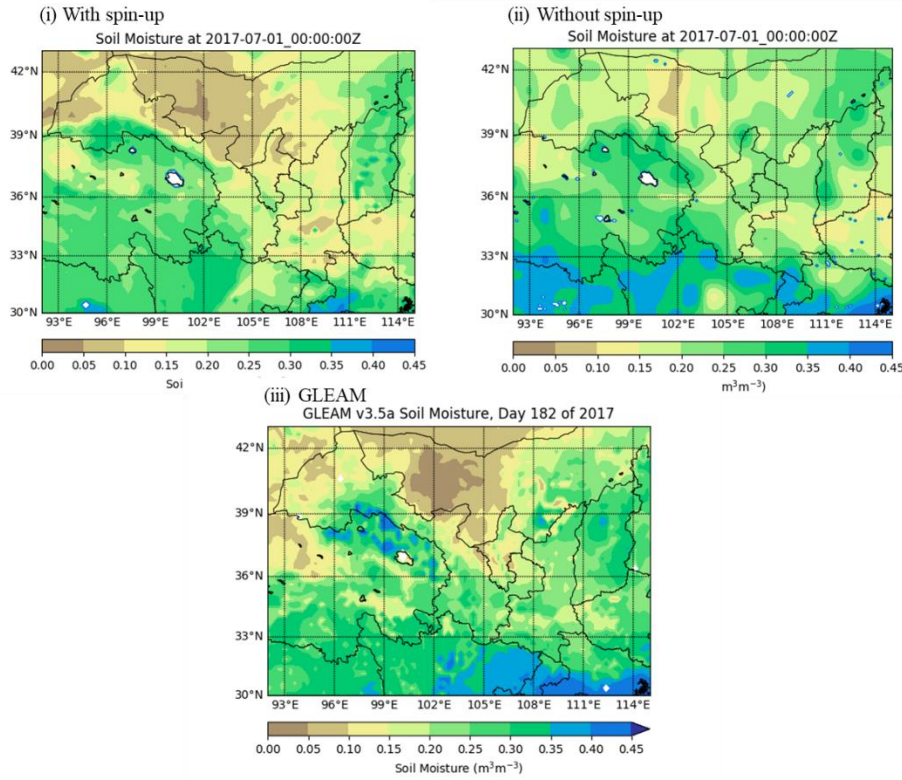


Figure 8. Soil moisture distribution on 1 July 2017 in the Northwest China domain in (top) spin-up case; (middle) right at model initialization without any spin-up; (bottom) GLEAM version 3.5a.

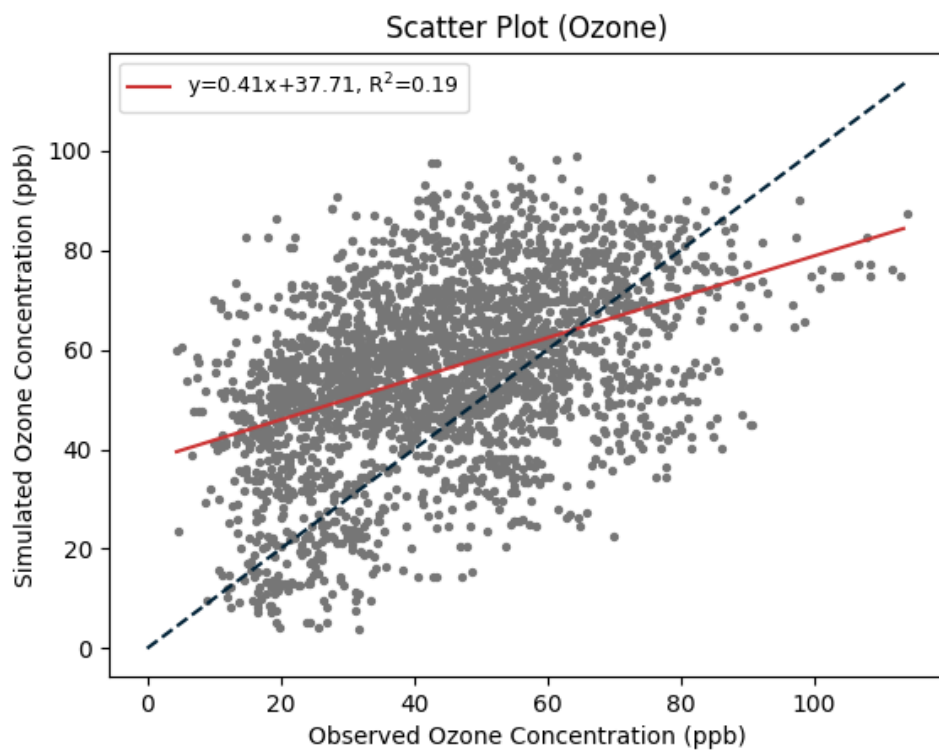
In general, the soil is drier in the spin-up simulation. It reduces the wet bias over Mongolia and part of Xinjiang. However, the simulation without spin-up gives better estimation over southern part of the domain (e.g., Sichuan and Hubei provinces). Overall, assuming the GLEAM dataset represents the ground truth, the spun-up soil moisture is slightly closer to the reality. The soil moisture field spun up is retained for future simulations based on its stability of the soil field in the model world.

2.3.3 Chemistry input

In terms of chemistry, two data sources including MOZART-4 and GEOS-Chem were investigated to quantify their differences in generating chemical initial and boundary conditions for the model. MOZART-4 provides simulation results such as species concentrations until January 2018, although it was decommissioned in 2010. The meteorological input is based on GEOS-5 and the emission inventories are dated back to 2011. The simulation results were used as chemical initial and boundary conditions for our model. Another set of chemical initial and boundary conditions was prepared using GC version 12.9.3. Modern-Era Retrospective analysis for Research and Applications, Version 2 (MERRA-2) (Gelaro et al., 2017) was chosen as the meteorological input and Harmonized Emissions Component (HEMCO) (Keller et al., 2014) was responsible for the emissions. The species concentrations and the collection that contains meteorological fields were used to generate another set of chemical initial and boundary conditions. Figure 9 shows the verification of MOZART-4 and GC against observations by taking the daily average of the species concentration and matching the site observations to the closest grid box. GC reduces the high-biases of simulated ozone concentrations as inferred from the smaller value of y -intercept of the fitting line. For emitted species such as NO₂, the validation results of both chemical transport models are comparable. Using GC to provide chemical initial and boundary condition improves the initialization of

generated species through better chemistry and meteorology representation.

However, accurately initializing emitted species remains challenging.



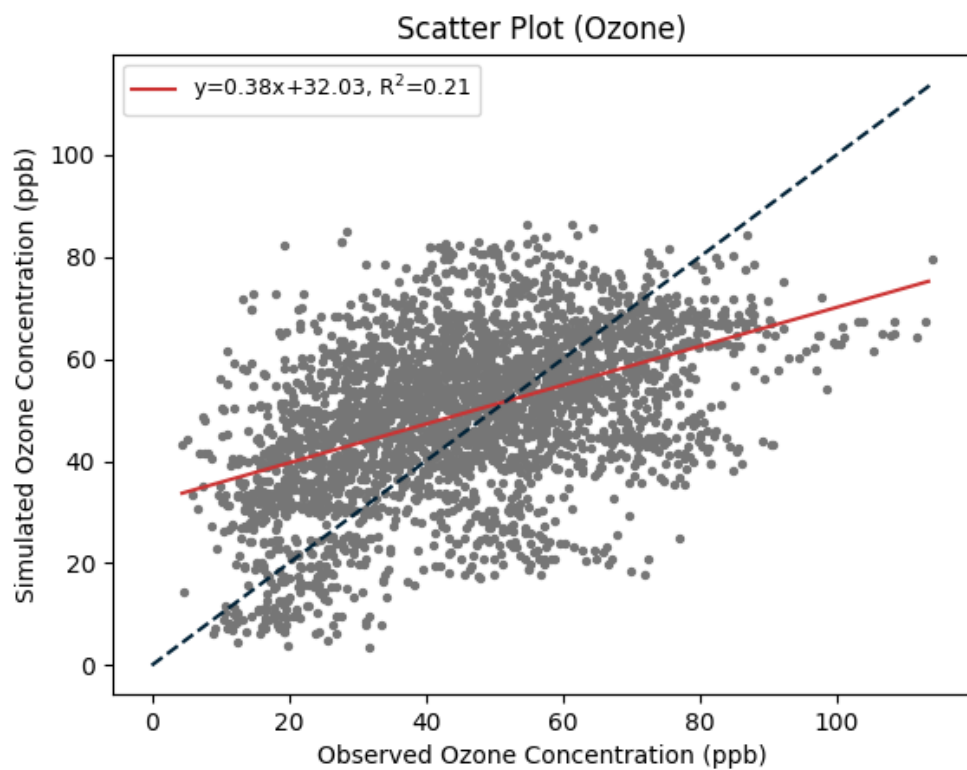


Figure 9. Scatter plot of (top) MOZART-4 and (bottom) GEOS-Chem (GC) simulated against observed ozone concentration averaged daily by observation sites. GC reduces the high-biases in ozone simulations compared with MOZART-4.

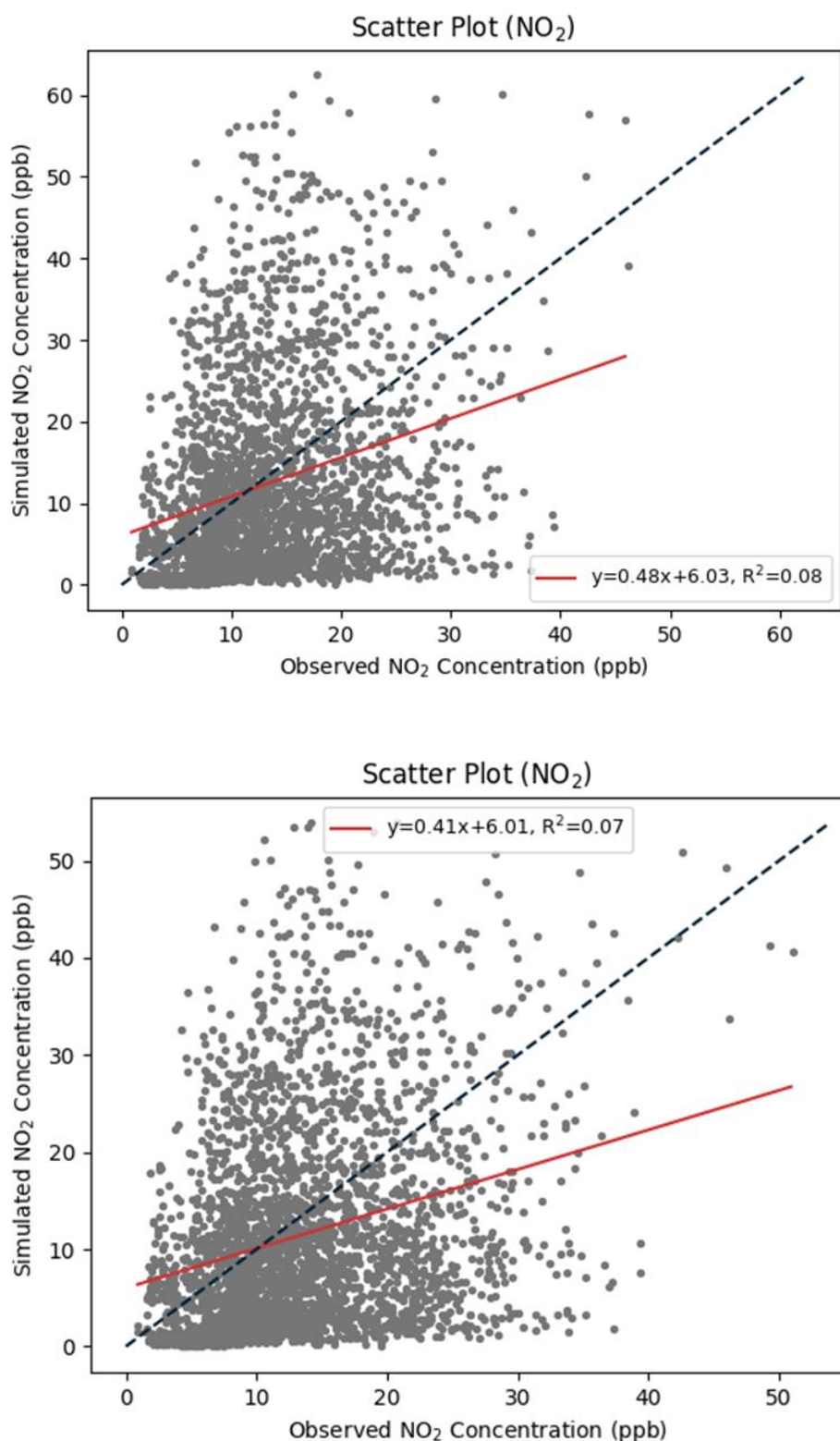


Figure 10. Scatter plot of (top) MOZART-4 and (bottom) GEOS-Chem (GC) simulated against observed NO₂ concentration averaged daily by observation sites. The performances of MOZART-4 and GC are comparable.

2.4 Crop distribution

Irrigation practices are also highly correlated with crop types and would eventually affect our simulations. In China, crops that are grown over extensive farmlands (e.g., wheat, rice, rapeseed) usually adopt furrow irrigation, which is a kind of surface irrigation similar to flooded irrigation. On the contrary, cash crops (e.g., cotton, potatoes, grapes) usually uses drip irrigation. These irrigation practices are results from irrigation water management and pricing. We used the crop functional type distribution of Community Land Model (CLM) version 5.0 (Lawrence et al., 2019) to investigate the common crops present in our Northwest China domain. Figure 11 shows the distribution of the most common crops.

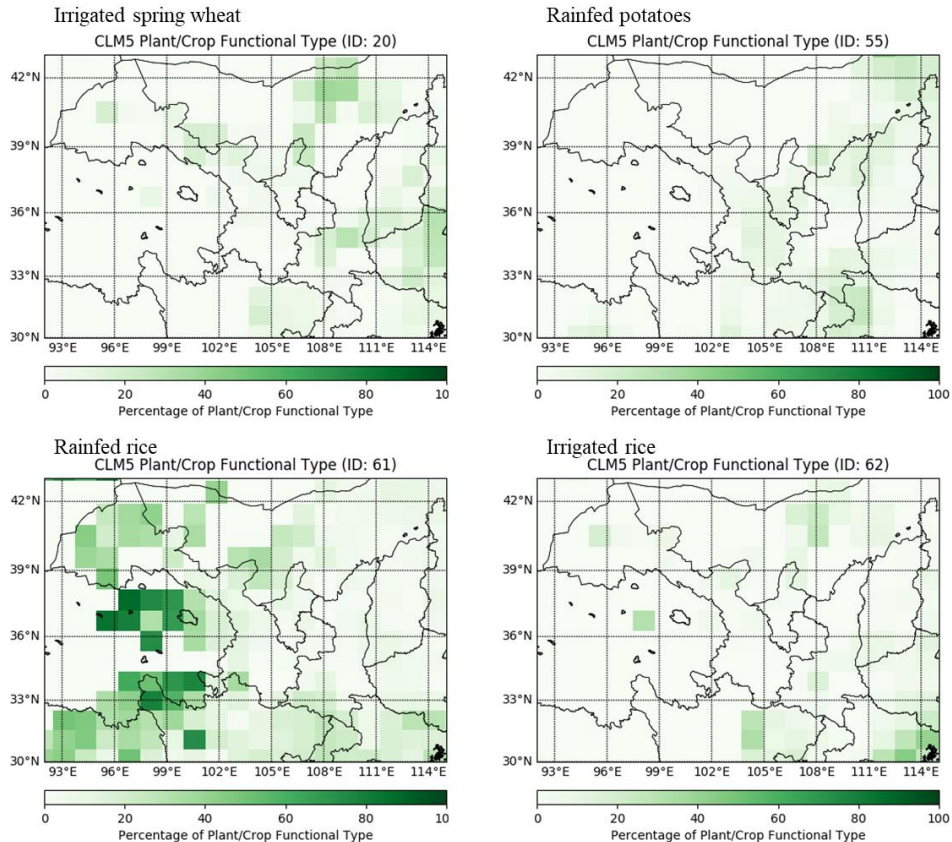


Figure 11. Most common crops present in our Northwest China domain as depicted by the crop functional type of Community Land Model version 5.0 (CLM5).

Most crops being grown in the domain are usually furrow irrigated, which matches with the dominating amount (94.0%) of surface irrigation implemented over China. A small proportion of potatoes are grown coinciding with the small proportion of irrigation that requires machinery (e.g., sprinkler and drip irrigation). It is noteworthy that in semiarid regions where rainfall and water are limited, irrigation technology develops faster in order to adapt to the climatic environment for improving water-saving irrigation strategies.

2.5 Site-level irrigation and its impacts to the surface

The impacts of irrigation in real life were studied using observations over farms that helps validate our model. In-situ measurement data from two farms in central Gansu was obtained. Both farms are mulched, one of them is irrigated with flooded irrigation and the other employs drip irrigation. The temporal resolution of the data is one day, and it is available in 2017 growing season that typically spans from May to September. Flux towers are installed in the site such that flux data including latent heat flux and sensible heat flux are available. The data also records the irrigation water used and other common meteorological variables. Irrigation practice and their effects to the soil of farm and surface weather can be determined.

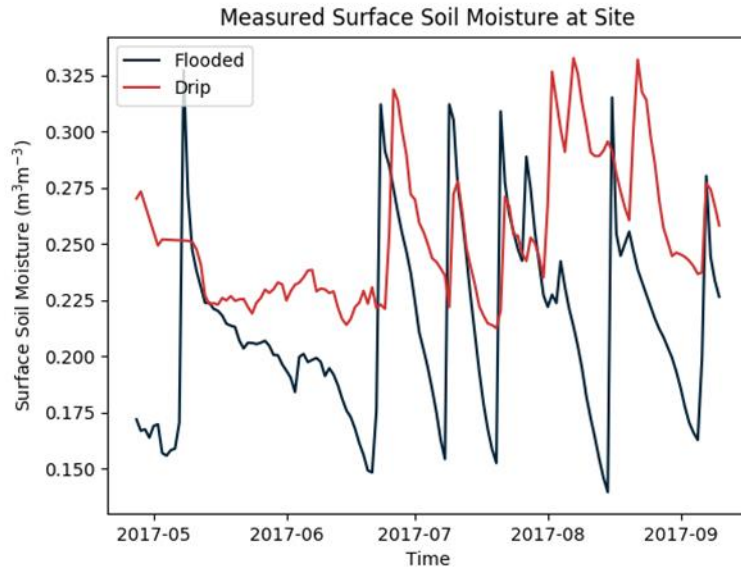


Figure 12. Time series of surface soil moisture from (blue) farm with flooded irrigation and (red) farm with drip irrigation. Irrigation is deployed when the surface soil moisture drops to a certain threshold.

The irrigation practice is different from Valmassoi et al. (2020), which assumed irrigation water to be applied daily. Instead, 錯誤! 找不到參照來源。 shows that irrigation is typically activated when the surface soil moisture drops to a certain threshold. This is a more trivial irrigation practice as farmers can save time and cost from irrigating the farmland that is not in water deficit. Consequently, irrigation is usually applied once every three weeks depending on the weather and the actual soil moisture availability. After each irrigation, the increment in surface soil moisture of the flooded irrigation case is higher than drip irrigation, suggesting that flooded irrigation applies more water. In this growing season, flooded irrigation used about 600 mm irrigation whereas drip irrigation only used about 300 mm. The amount of irrigation water used in flooded irrigation is constant whereas it varies in each drip irrigation because the implementation of the pipe network over the farm allows a more flexible irrigation amount taking the crop deficit in water into account.

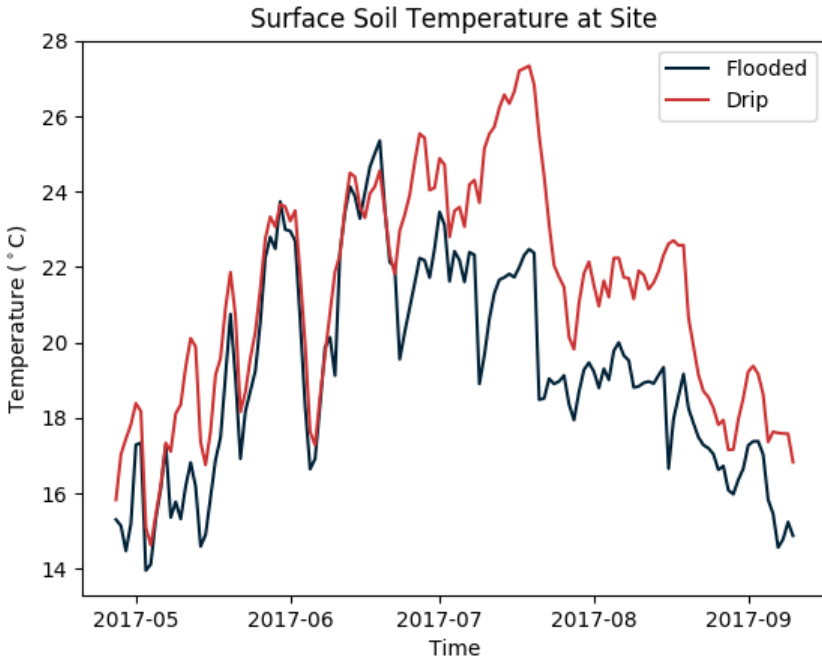


Figure 13. Time series of surface soil temperature from (blue) farm with flooded irrigation and (red) farm with drip irrigation. In general, the soil temperature is lower over the farm with flooded irrigation.

Figure 13 shows the time series of surface soil temperature of the two farms. Due to the higher amount of irrigation water applied, the surface soil temperature in the flooded case is lower than the drip case. The average surface soil temperature within this growing season of the flooded (drip) case is 18.9°C (21.1°C), of which the flooded case is 2.2°C lower than the drip case. The difference in temperature grew with time within this season because irrigation was less applied during the first two months in view of the moisture availability that caused such difference to be less prominent when the season just began.

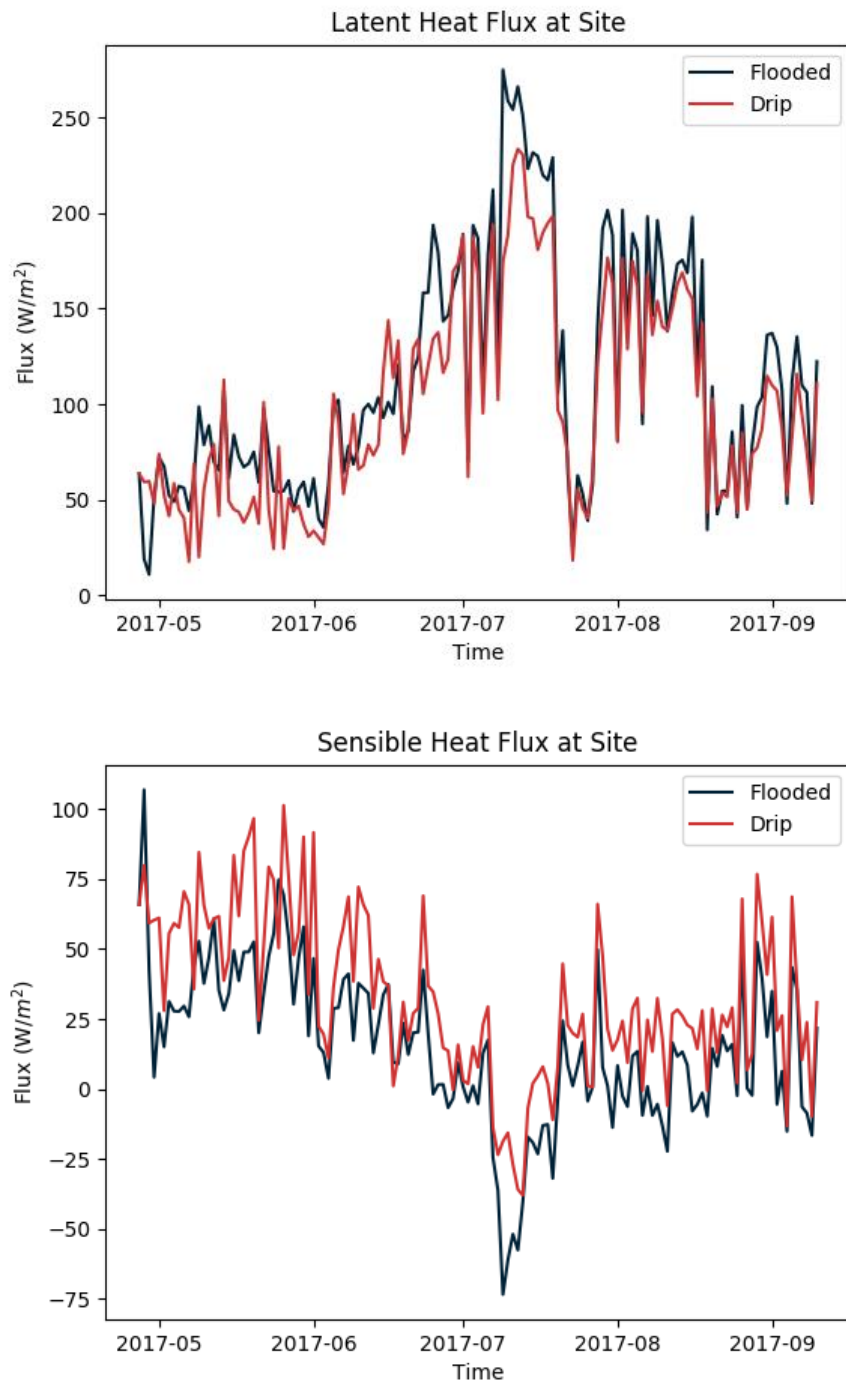


Figure 14. Time series of (top) latent heat flux and (bottom) sensible heat flux from (blue) farm with flooded irrigation and (red) farm with drip irrigation. Latent heat flux (sensible heat flux) is higher (lower) in the flooded case compared with the drip case.

The extra water applied in the flooded case also affects latent heat flux and

sensible heat flux. Figure 14 shows that the near surface moisture gradient steepens more substantially in the flooded case such that the latent heat flux of flooded case is higher than the drip case by 14.2 W m^{-2} . On the contrary, the sensible heat flux of flooded case is lower because of the drop in surface temperature that reduces the temperature gradient. It is lower than the drip case by 18.6 W m^{-2} , comparable to the magnitude of increase in latent heat flux in view of surface energy balance. The minute imbalance in these two magnitudes may be attributed to the slightly different position of the two sites that do not receive the same amount of net radiation, and there are also changes in the ground heat flux that is also dependent to the temperature gradient.

3. Results and discussion

3.1 Hypothetical experiments

Before running any realistic simulations as mentioned in chapter 2, hypothetical simulations where irrigation is applied in all the grid cells in the domain at all times were first tested using Noah LSM and Qinghai province as the domain. It is found that soil moisture increases most in the hypothetical flooded irrigation experiment as expected (Figure 15). Drip irrigation causes minimal change in soil moisture compared with the “control run”, which is the simulation without any implementation of irrigation schemes into the LSM. Since sprinkler irrigation is simulated by adding artificial precipitation, the irrigation water at the surface is easier to be evaporated into the atmosphere by sunlight or surface wind.

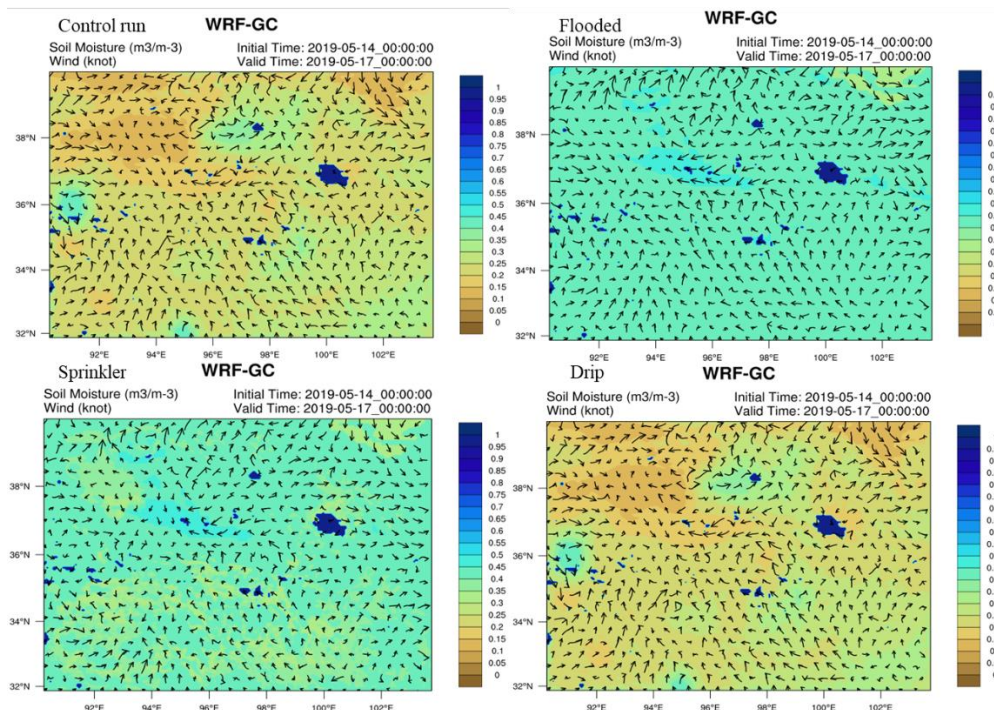


Figure 15. Soil moisture at the time three days after the initial condition of control run, hypothetical flooded irrigation, sprinkler irrigation, and drip irrigation. The arrows represent 10-m wind field.

While the change in soil moisture is the most observable in hypothetical flooded irrigation case, the most prominent change in weather is indeed found in the sprinkler case because of highest amount of water evaporated into atmosphere. The 2-m air temperature has the highest decrease (Figure 16) while cloud fraction has the highest increase compared with the control run (Figure 17). Simulation with drip irrigation implemented is very similar to the control run, since irrigation water added is immediately transpired leaving no extra water left in the grid cell. However, the concentration of chemical species such as NO_x differs because of alterations in land-atmosphere fluxes that affect production of chemical pollutants.

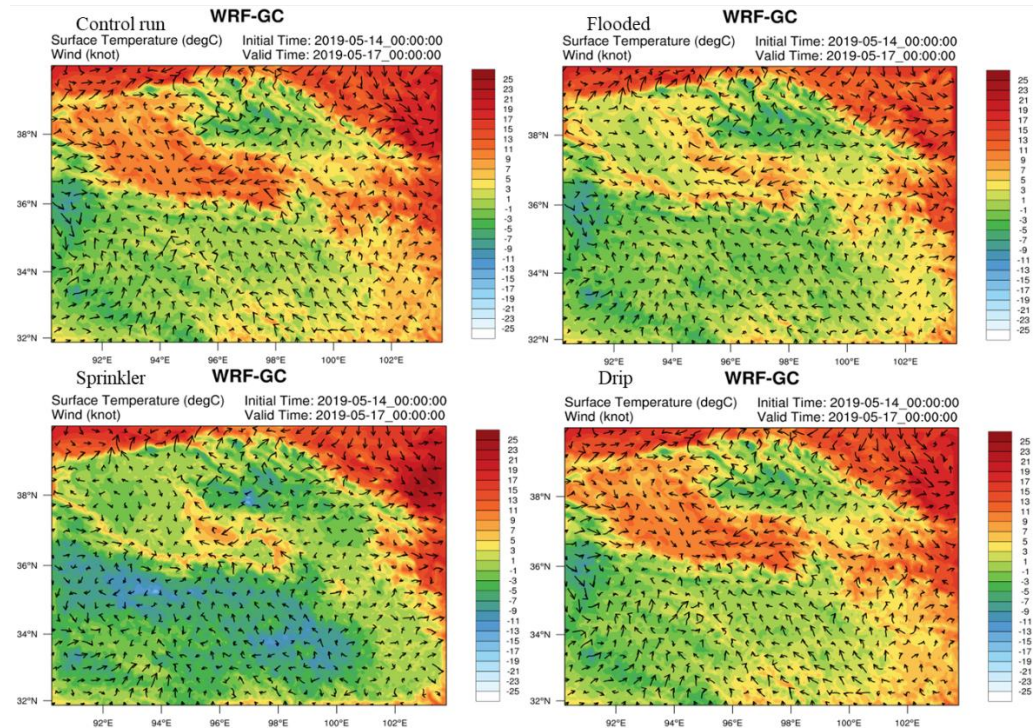


Figure 16. 2-m air temperature at the time three days after the initial condition of control run, hypothetical flooded irrigation, sprinkler irrigation, and drip irrigation. The arrows represent 10-m wind field.

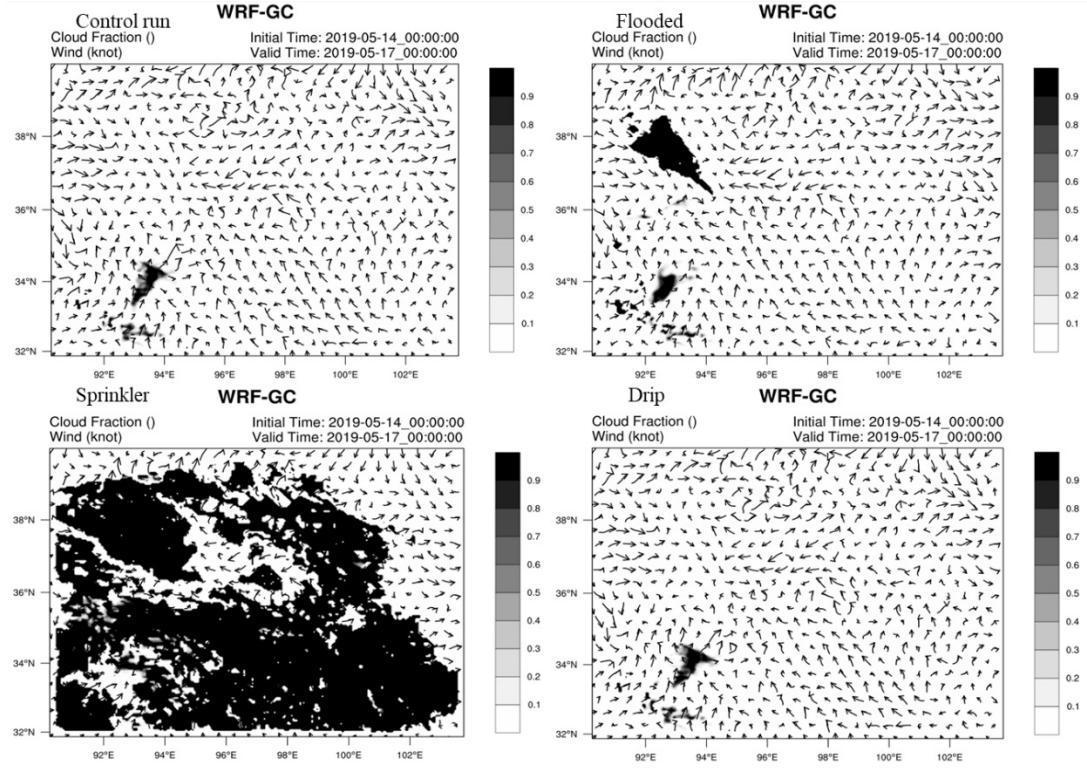


Figure 17. Cloud fraction at the time three days after the initial condition of control run, hypothetical flooded irrigation, sprinkler irrigation, and drip irrigation. The arrows represent 10-m wind field.

3.2 Production simulations

3.2.1 Regional weather modification

Having confirmed the results of hypothetical experiments are in-line with theoretical anticipations, the irrigation mechanism in the model was modified to be more realistic, which is to apply water at certain times, over irrigated cell from FAO, and whether there is a demand for irrigation according to actual soil moisture content. In the production simulations, Figure 18 shows that although both Henan and Hebei provinces are equipped with irrigation, Hebei province is actually not irrigated. This is attributed to the soil moisture abundance in different regions such that Hebei province is not considered to be in irrigation demand. From the BNU soil map, the dominant soil type in Henan province is clay loam, while it is loam for

Hebei province. Physically, clay loam has a higher wilting point, which means there is a higher proportion of water that is not accessible by crops. In other words, if the soil moisture content between Henan and Hebei provinces are similar, there is a greater demand to irrigate because water accessibility in Henan province is lower, as depicted by the higher wilting point.

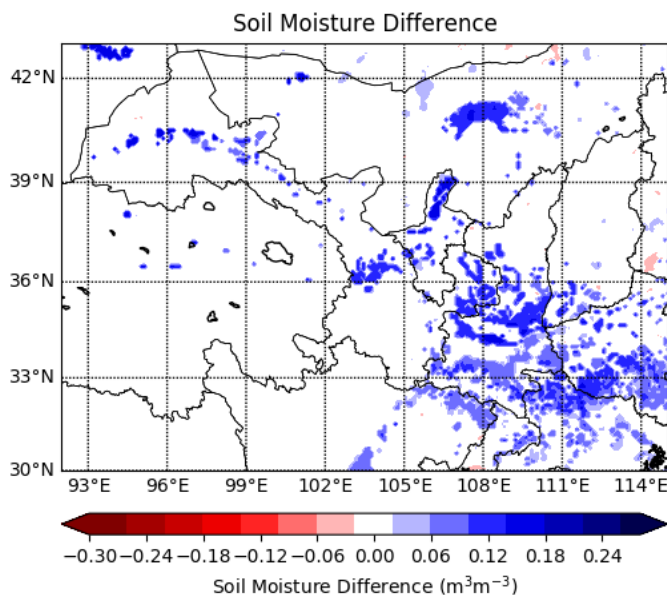


Figure 18. Soil moisture difference of flooded irrigation compared with control run.

The increase in soil moisture represents the regions that are irrigated according to FAO irrigation mask and the irrigation threshold. Some regions equipped with irrigation are not irrigated in the model because the soil moisture does not fall below the irrigation threshold.

It is found that both flooded irrigation and sprinkler irrigation can cause a drop in 2-m air temperature, while drip irrigation has negligible effect on temperature. Figure 19 shows the averaged temperature differences between the control run and a particular irrigation scheme during July 2017. Flooded irrigation

causes the most substantial temperature decrease, with magnitude up to about 2°C in some parts of Shaanxi and Hubei provinces. Sprinkler irrigation causes a slightly smaller temperature drop. With more irrigation water infiltrated into the soil through flooded irrigation, the heat capacity of the soil would increase. This would help moderate soil temperature, thus reducing the increase in temperature during daytime. On the contrary, sprinkler irrigation adds water in the form of precipitation in the LSM, such that less infiltration into the soil is anticipated. The extra amount of water on the surface can be more easily carried away by surface processes; for example, surface moisture can be transported by wind or evaporated when there is strong heating during a sunny day. There is no observable change in 2-m air temperature if drip irrigation is adopted. For drip irrigation, it adds the least amount of water. In particular, it is achieved by modifying the evapotranspiration in the LSM to mimic the fact that drip irrigation is capable to add the near exact amount of water that the crop intercepts. Our simulation results are in accordance with those based on physical arguments. The simulated temperature drop is comparable to similar studies. For example, Zhang et al. (2017) implemented irrigation into WRF and found that daily mean temperature drops by 1.7 °C. Li et al. (2016) used WRF-Chem to study irrigation over the Central Valley of the United States and found that irrigation would cause temperature drop of about 2 °C.

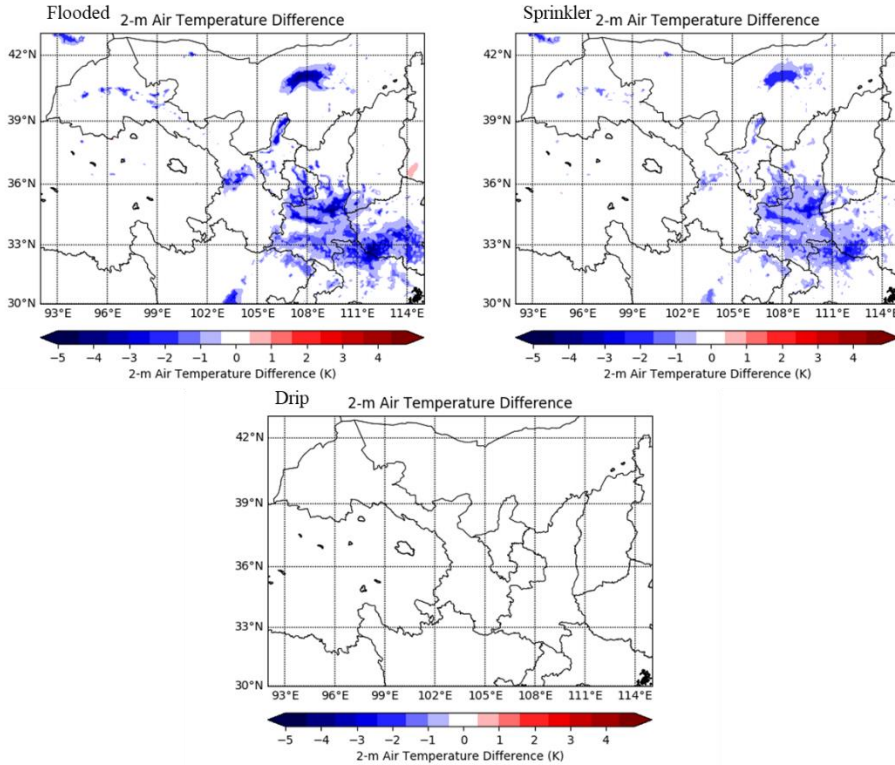


Figure 19. 2-m air temperature difference of flooded irrigation, sprinkler irrigation, and drip irrigation compared with the control run (without irrigation).

Surface fluxes including sensible heat flux and latent heat flux play important roles in energy partitioning that affects regional weather. Overall, irrigation (except drip irrigation that has merely no effect) can reduce sensible heat flux and increase latent heat flux. Figure 20 shows the change in the latent heat flux of sprinkler irrigation as an example. Reduction in sensible heat fluxes over irrigated grid cells is related to the drop of surface and air temperature, which decreases vertical temperature gradient and hence inhibits convective activities and mixing. On the contrary, the rise in latent heat flux is related to the increased moisture gradient. The magnitude of the decrease in sensible heat flux is comparable to the increase in latent heat flux as shown in Figure 21, which is expected based on surface energy balance conservation. The simulated change in fluxes is of the same order of magnitude

compared with Zhang et al. (2017). A decrease in sensible heat flux and thus convective mixing also causes the planetary boundary layer (PBL) height to decrease. Flooded irrigation causes PBL height to decrease by about 700 m in the eastern part of the domain, greater than the amount of drop of about 300 meters if sprinkler irrigation is used. The PBL is vital to infer vertical mixing of pollutants emitted or generated near the surface that in turn affect air quality.

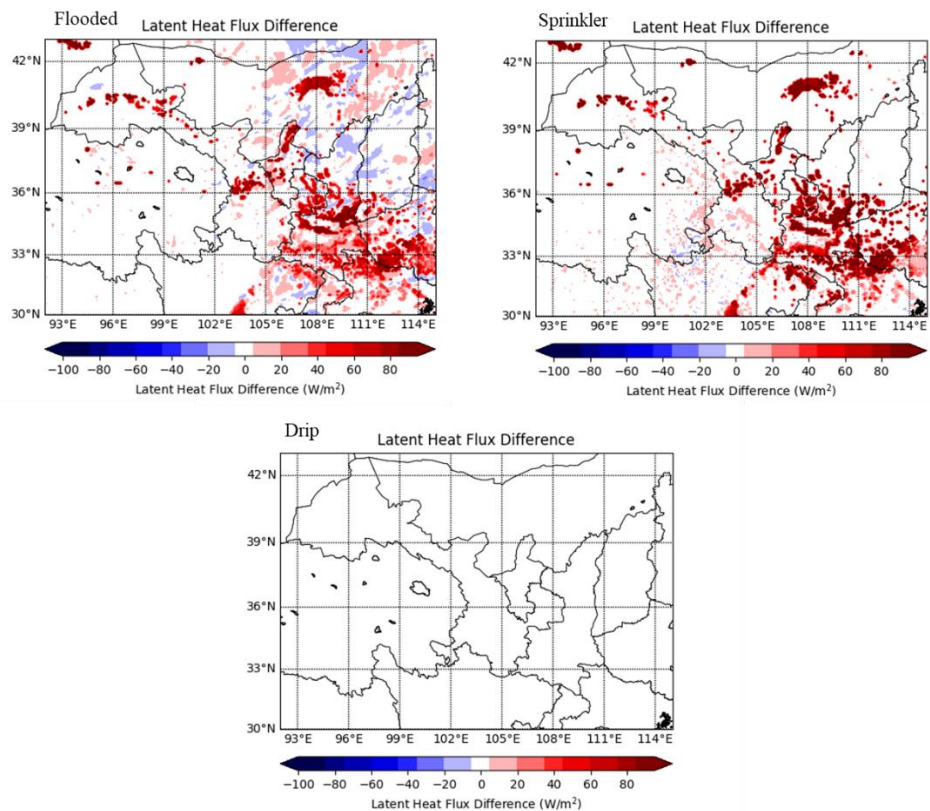


Figure 20. Latent heat flux difference of flooded irrigation, sprinkler irrigation, and drip irrigation compared with the control run.

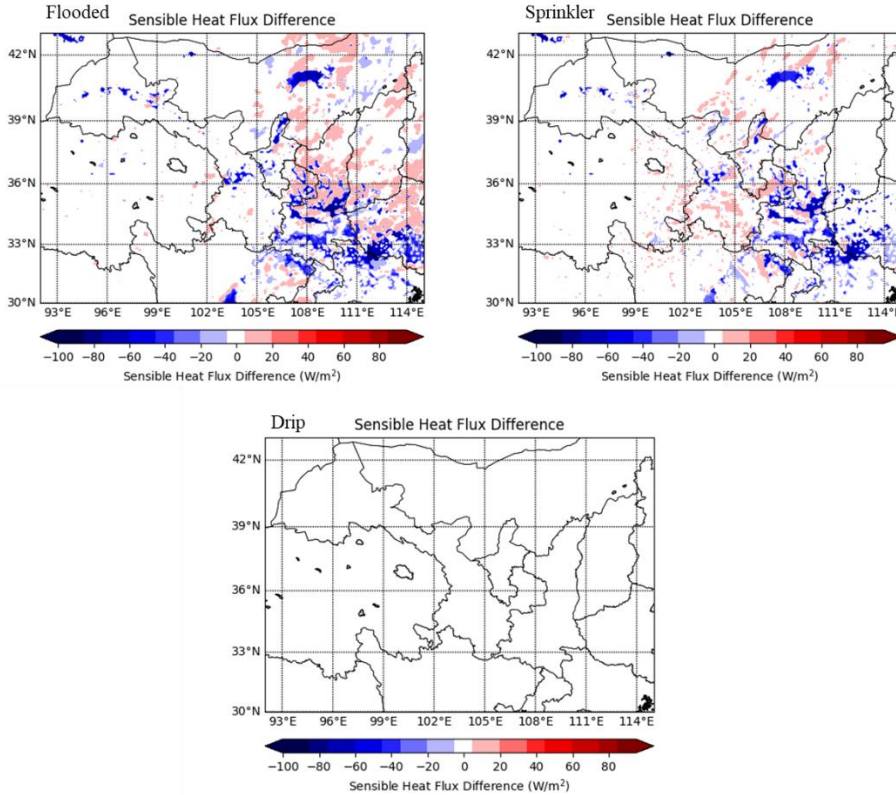


Figure 21. Sensible heat flux difference of flooded irrigation, sprinkler irrigation, and drip irrigation compared with the control run.

Since the surface is cooled, the air parcel becomes denser and eventually accumulates to build a higher surface pressure. Atmospheric stability also improves associated with the higher pressure as air tends to descend to inhibit convective activities, which agrees with the lowered PBL height. Changes in surface pressure would then alter the surface wind field. Figure 22 shows the changes in surface pressure and wind field. Surface divergence depicted by the diverging 10-m u -component and v -component of wind can be observed wherever a relative high surface pressure builds up. From the change in surface wind vector plots, surface wind diverges from a few irrigation centers including Xi'an of Shaanxi province, central Gansu province, and Henan province. Air parcels diverge from these irrigation centers and are advected by the surface high pressure to the surroundings.

Since the weather is more stable over irrigated cells, the modified surface wind field would advect the moistened, stabilized air parcel to the vicinity. These modifications are also subjected to the terrain nearby in which higher terrain may confine the modified air parcel in its original position, such as the Gansu province irrigation center cannot further push air parcels to the west due to the higher terrain of Qinghai province.

It is worth to note that whether implementation of flooded irrigation would improve the simulations by minimizing the errors compared with observations. Since flooded irrigation largely dominates the irrigation systems in China, theoretically the flooded irrigation simulation should represent the simulation better. Figure 23 shows the validation of flooded and control simulations with observed 2-m air temperature data. Flooded irrigation substantially reduces the high y -intercept and slightly higher slope such that simulations with irrigation are represent the real world better.

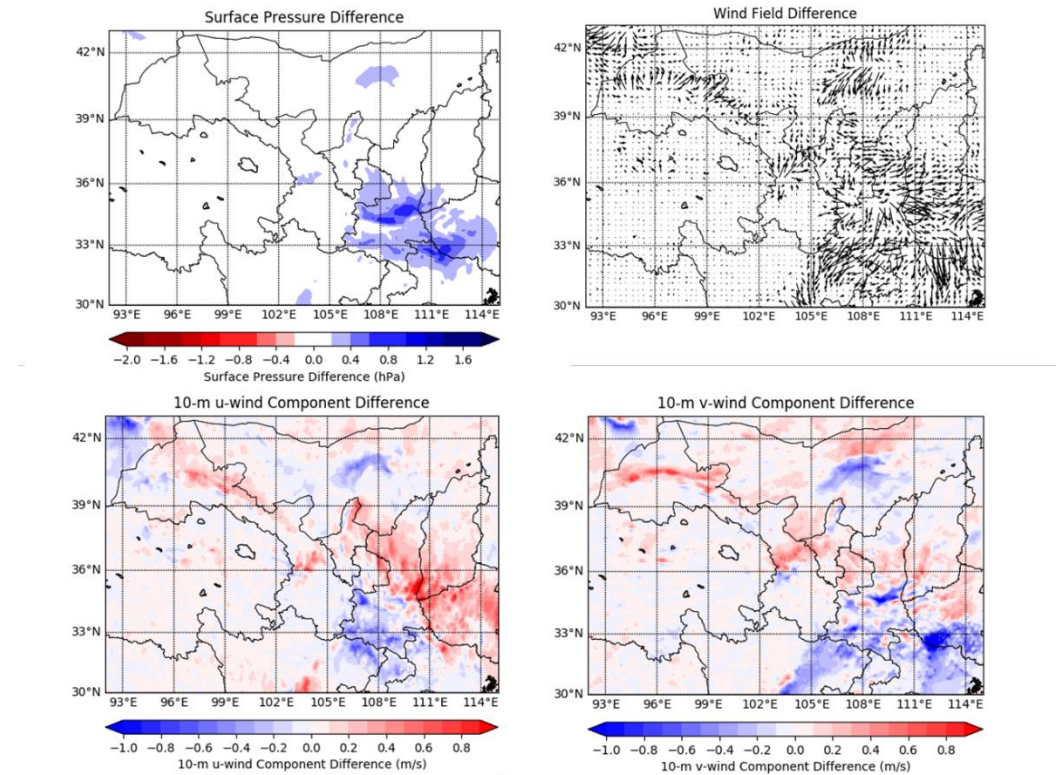


Figure 22. Changes in surface pressure, wind field, 10-m *u*-wind component, and 10-m *v*-wind component of the flooded irrigation case compared with the control run.

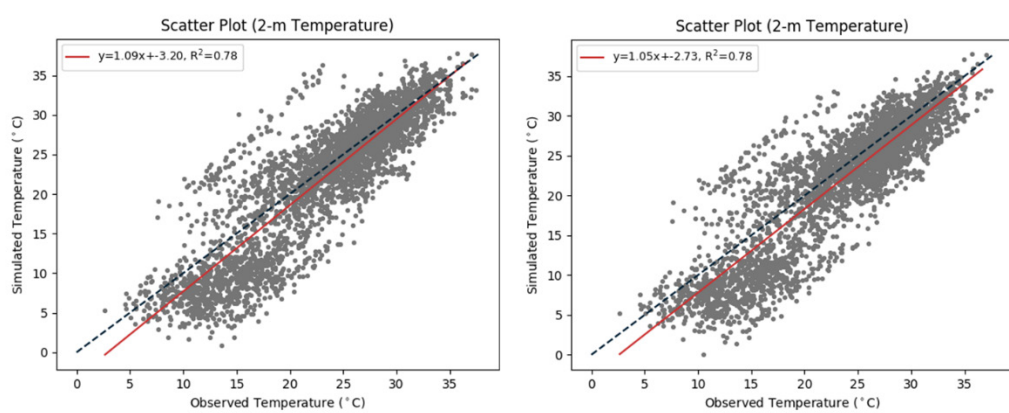


Figure 23. Scatter plot of (left) control and (right) flooded irrigation simulation against observation.

3.2.2 Regional air quality modification

Other than modifying regional weather, air quality is also altered based on the change in weather. Since turbulent intensity and vertical mixing are reduced by the lowered surface temperature and convection, air pollutants such as NO_x , CO, ozone, $\text{PM}_{2.5}$ are more concentrated at the surface. Figure 24 shows the change in surface NO_x . They generally increase over irrigated grid cells, with most degraded air quality in the flooded irrigation experiment. This is consistent with the fact that the reduction in PBL height is most substantial in this case. Air quality worsens the most as NO_x concentration increases up to 6 ppb in irrigated regions. As mentioned earlier, although drip irrigation does not contribute to observable change in regional weather, here regional air quality is slightly affected but the deterioration is still minimal.

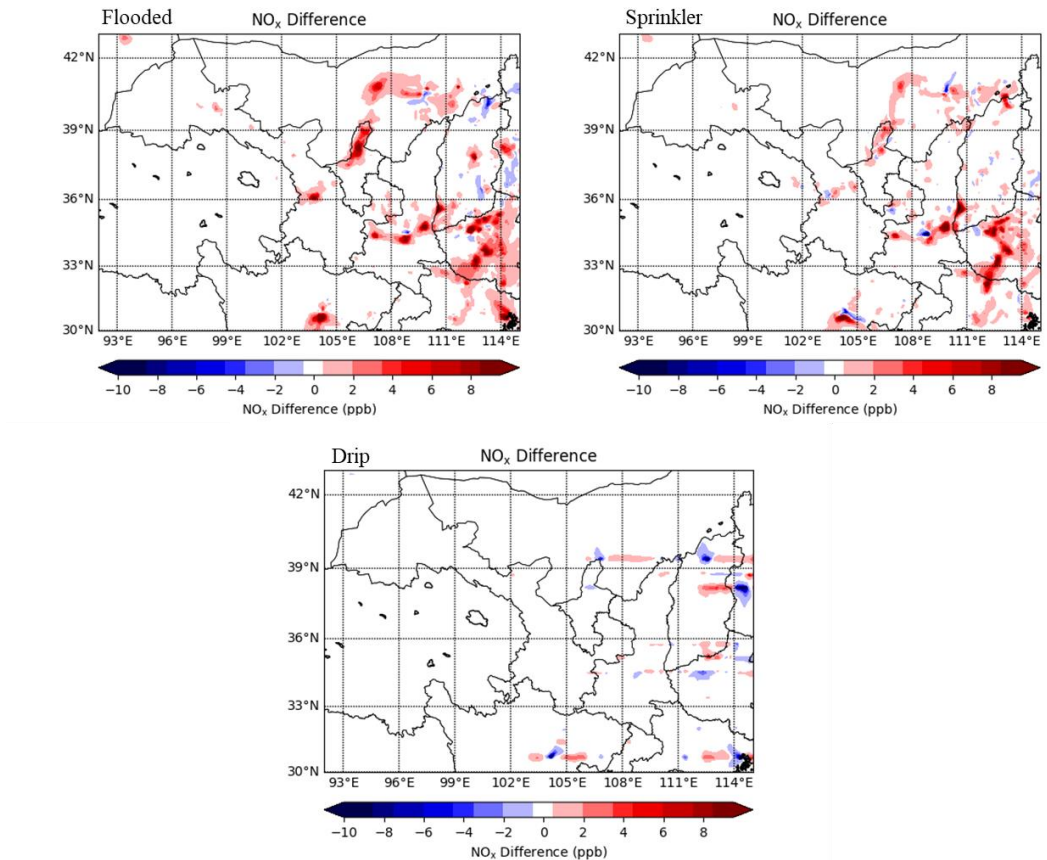


Figure 24. Change in NO_x concentration of flooded irrigation, sprinkler irrigation, and drip irrigation compared with control run.

Surface ozone is a hazardous air pollutant to human health and causes damages to global crop yields (Wang et al., 2020). Unlike NO_x that is mostly emitted by combustions, ozone is generated by photooxidation of various precursors such as carbon monoxide (CO), volatile organic compounds (VOCs) and NO_x . Ozone genesis is also sensitive to temperature and sunlight. These dependencies have increased the difficulty of accurately simulating ozone concentration. Here we find that the impacts of irrigation on ozone concentration in the domain are mixed. Figure 25 shows the changes in ozone concentration. Ozone concentration decreases or changes by a little amount over irrigation centers. The substantial increase in NO strengthens the titration effect on ozone, which is to remove ozone through chemical

reaction with NO. PM_{2.5} also scavenges NO_x such that ozone is less generated (Li et al., 2020). Our simulation results show that both NO_x and PM_{2.5} increases over irrigated cell such that less ozone should be produced. Meteorologically, the surface high pressure induced by irrigation cooling also pushes ozone precursors away from Hubei and Henan provinces, but the relatively high terrain in southeastern Shaanxi province prohibits NO from further being transported into the central Shaanxi province. In the absence of the increase in NO but with stabilized weather, ozone concentration thus increased over most parts of Shaanxi province. On the other hand, its surroundings are benefited from decreased ozone concentration. Results show that ozone concentration increases by up to 6 ppb, comparable to Li et al. (2016) that simulated a 4 ppb increase. The region that experiences an increase in NO_x is more confined to the emission position due to its lower residence time than ozone.

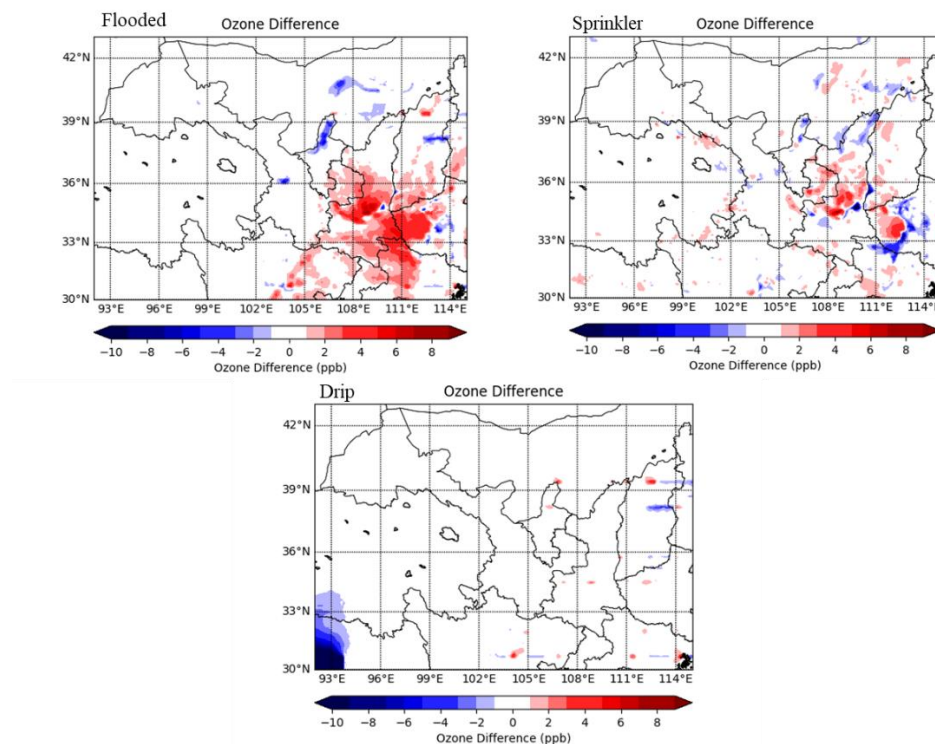


Figure 25. Change in ozone concentration of flooded irrigation, sprinkler irrigation, and drip irrigation compared with control run.

3.3 Vertical structure

After investigating the modification of air quality and PBL, examining the vertical profiles can provide more insights about vertical mixing. Data of irrigated grid cells located near Xi'an of Shaanxi province over daytime was extracted to examine the vertical profiles of various parameters. Using the hybrid sigma-eta vertical coordinate with the top pressure defined in the model to be 10 hPa, eta value of 0.8 is an approximation to about 1500 m above ground level. Figure 26 shows the vertical profiles of mixing ratio and potential temperature of the control run and different irrigation schemes. The near surface mixing ratio increases slightly but the effects diminish in the lower troposphere. More importantly, the gradient of potential temperature increases in flooded irrigation case with a lowered surface potential temperature, implying a more stable atmosphere. The cooling effect due to irrigation is up to about 1500 m above ground level.

Figure 27 shows the modification to the vertical structures of air pollutants. Flooded irrigation increases surface NO_x concentration by about 0.6 ppb (12%). For CO, flooded irrigation also causes more deterioration to air quality, raising surface CO concentration by about 22 ppb (10%). No obvious change in lower tropospheric NO_x is found with irrigation implemented, but flooded irrigation greatly reduces the amount of CO in the lower troposphere. Figure 28 shows the vertical profile of ozone, which is different from the emitted species. The maximum ozone concentration is found in the lower troposphere instead of at the surface since ozone is not emitted at the surface. Irrigation causes PBL height to descend, thus the height of maximum ozone concentration in flooded irrigation simulation is lower than the others. Near surface ozone removed by meant of titration by other chemical species or dry deposition by plants. Since the vertical profiles are averaged over irrigated

cells of southern Shaanxi province, surface ozone increases if flooded irrigation is implemented as shown in Figure 25, but there are indeed some regions with decreased surface ozone because of the advection of precursors. Overall, both modifications to weather and air quality are confined to the lower troposphere as the irrigation water in the LSM mostly affect the surface and lower troposphere through surface heat and moisture fluxes.

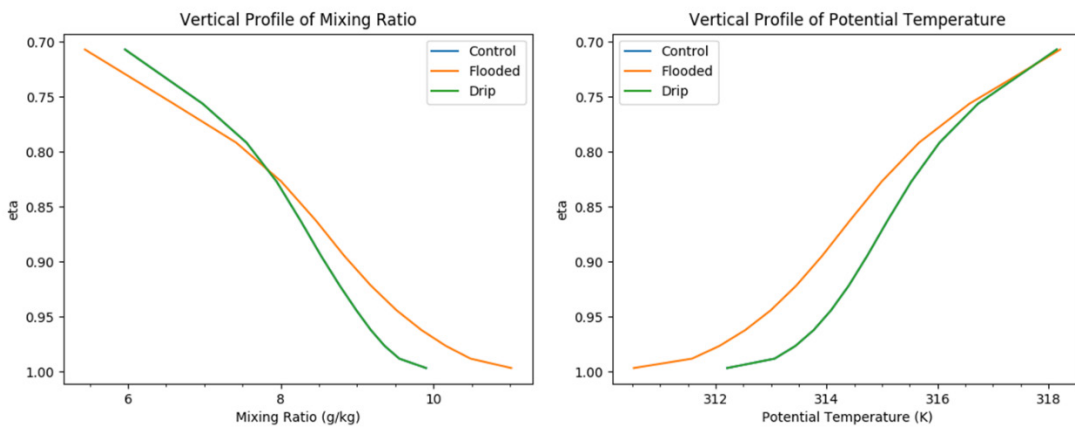


Figure 26. Vertical profiles of (left) mixing ratio, (right) potential temperature as simulated for irrigated grid cells near Xi'an of Shaanxi province over daytime.

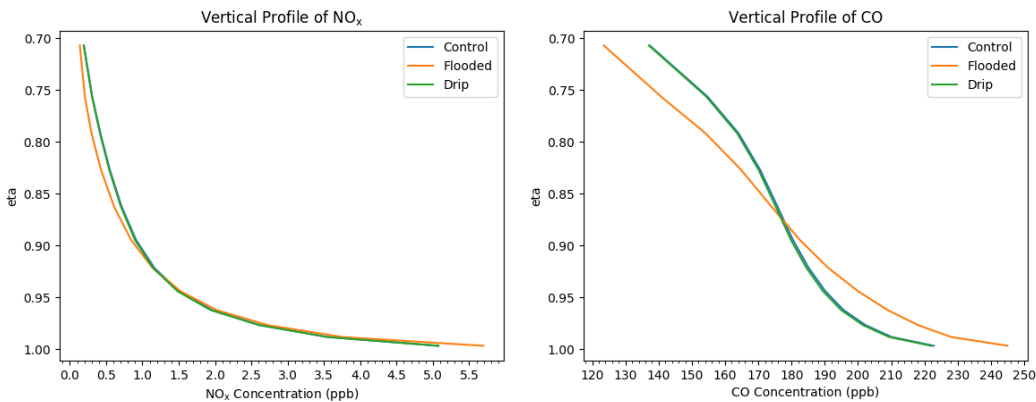


Figure 27. Vertical profiles of (left) NO_x, (right) CO as simulated for some irrigated grid cells near Xi'an of Shaanxi province over daytime.

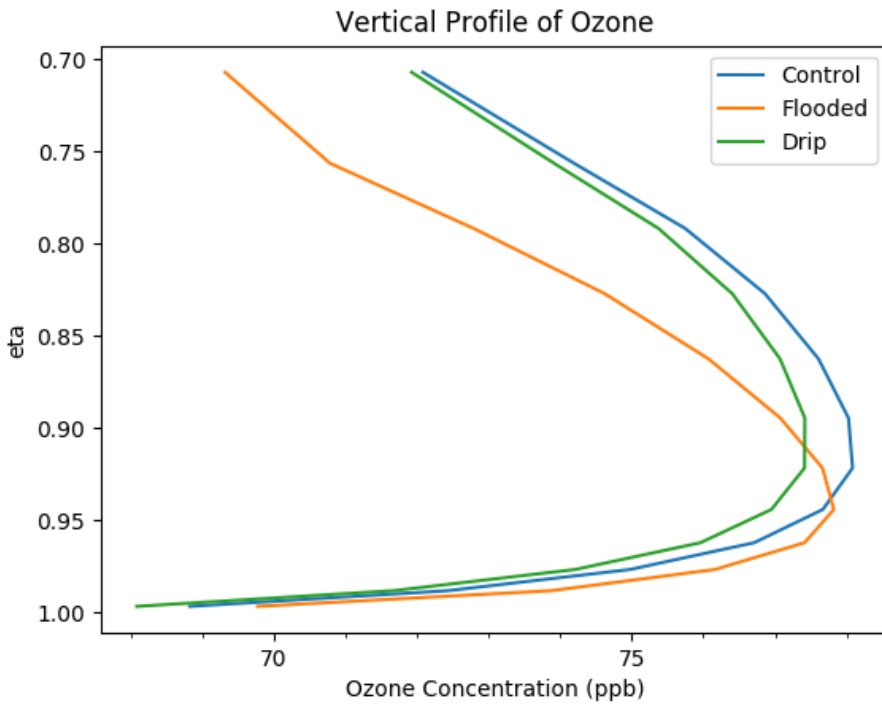


Figure 28. Vertical profile of ozone as simulated for some irrigated grid cells near Xi'an of Shaanxi province over daytime.

3.4 Site-level time series comparison

After understanding that flooded irrigation matches with the observations slightly better, it is also worth to examine the improvements of simulations in matching the observations of sites. The observation sites include those from WMO and CNEMC that have been introduced in chapter 2. Sites near southern Shaanxi province especially Xi'an were taking for verification because that is a heavily irrigated region in our model. Otherwise, from the previous figures, there is no observable change in weather and air quality over regions that are not irrigated in general. Figure 29 shows the 2-m air temperature time series of observation and simulations of a weather station near Xi'an, Shaanxi province. Flooded irrigation simulates better the real world as it is closest to the observation. Quantitatively, the mean absolute error of both control and drip run is 1.95°C , and the mean absolute error of flooded irrigation run is 1.63°C . For this station, flooded irrigation partially

corrects the high bias in temperature and reduces the error by about 20%.

In contrast to simulating weather such as temperature, WRF-GC or in general chemical transport models such as GEOS-Chem, WRF-Chem in simulating species concentration are not as skillful as simulating weather. Figure 30 shows the time series of simulated and observed species concentrations in an air quality station near Xi'an. The model fails to capture the actual value of the species concentration, but the simulated trend is in fair agreement in simulating CO. For NO₂ and CO, flooded irrigation gives the best estimation because the observed trend is a lot higher than the simulated trends, and flooded irrigation simulates the worst air quality because of stabilized weather. The simulation errors of ozone is different from the emitted species like NO₂ and CO. Although it has the most accurate simulated concentration, it does not show a consistent bias as the observation can either be higher or lower than the simulated values, which is not the case for the emitted species. This unskillful simulation of species concentration is indeed also observed when WRF-Chem is used as demonstrated by Li et al. (2016). Their simulation performance varies greatly among stations. While ozone is still better simulated, simulated CO differs from the observations by hundreds of ppb (equivalent to about 70%), and NO_x differs by tens of ppb (equivalent to about 40%).

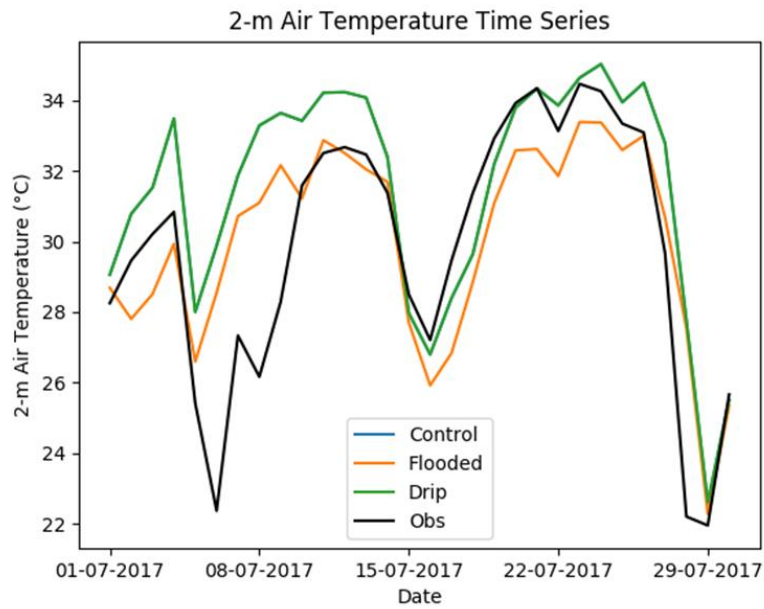


Figure 29. 2-m air temperature time series of observation and simulations at a weather station located near Xi'an, Shaanxi province (34.4N, 108.8E). Simulation of flooded irrigation matches with observations better than the others.

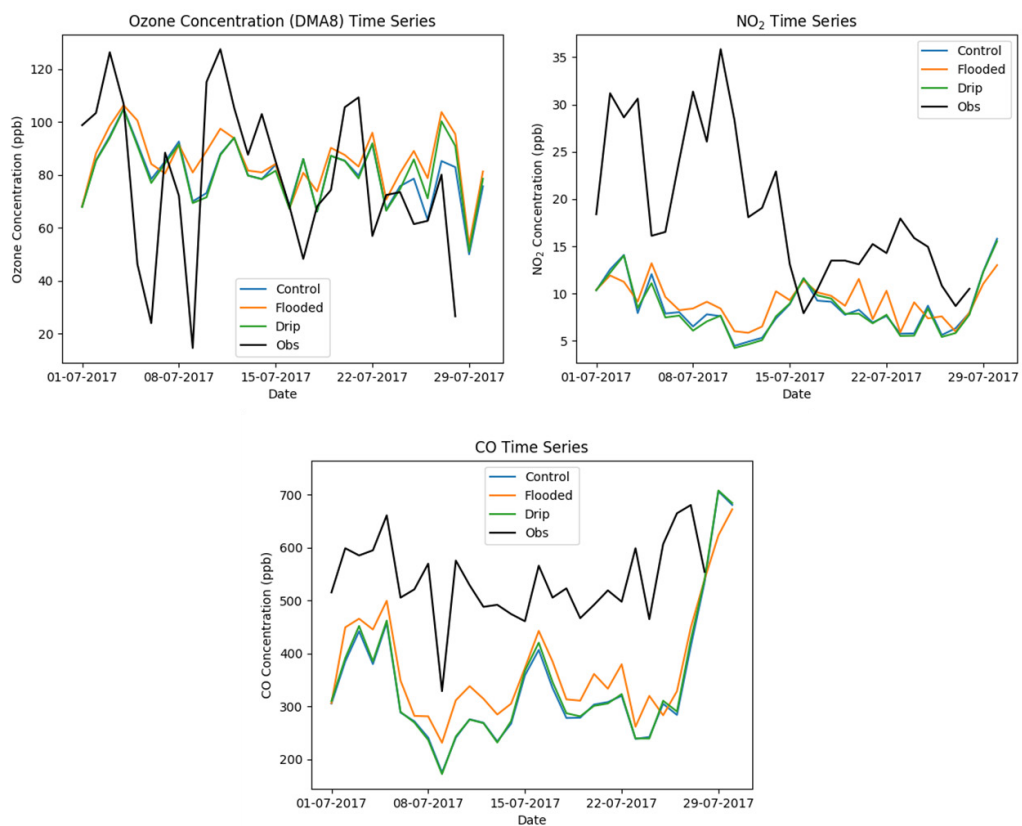


Figure 30. Time series of observed and simulated ozone (daily maximum 8-hourly average, DMA8), NO₂, and CO in a air quality observation site near Xi'an.

Compared with the simulated 2-m air temperature, our simulations cannot capture the actual value of species concentrations well yet the trend is in fair agreement for NO₂.

Simulating atmospheric chemistry is a lot more challenging than weather because of (i) inaccuracies in initial and boundary conditions; (ii) emission inventory uncertainties; and (iii) very high spatial dependence of species concentration.

Meteorological input is usually from reanalysis, which has a long history and good data assimilation techniques to provide best estimates for weather, whereas chemistry input relies on both weather and other chemical reactions. Emitted species such as NO_x depends a lot on parameterizing the emission, at the same time observation depends a lot on the surrounding environment such as density of human activities. Due to low residence time of NO_x, it usually confines to the emitted spots thus midget spatial difference can cause substantial errors. Species like ozone depends on various factors such as precursors concentrations, sunlight, temperature thus may suffer from error accumulations in different aspects with their own difficulties to capture accurately.

In view of the above results, we suggest drip irrigation to be the most preferable option to irrigate over semiarid Northwest China. From the field data, drip irrigation saves about 50% of irrigation water compared with flooded irrigation. It demonstrates a substantial water-saving potential because 94% of irrigation in China makes use of surface irrigation techniques. In terms of the meteorological impacts, drip irrigation causes minimum impacts to regional weather and climate, with no observable change in 2-m air temperature and surface wind field. If flooded irrigation is adopted instead, there is substantial cooling that stabilizes the weather, causing

hazardous air pollutants such as NO_x, ozone to increase near surface. The worsened air quality would affect both people and crops, which may in turn affect crop yield. Although the construction cost of flooded irrigation is substantially lower than drip irrigation, there are indeed other costs that are not considered and are revealed in the above simulations.

4. Conclusions and future work

Irrigation water usage is particularly important in semiarid regions such as Northwest China due to water shortage. Flooded irrigation, which is the traditional way of irrigation is the most dominant irrigation type in China yet water demanding. We took the modeling approach to investigate the impacts of different irrigation schemes to regional weather and air quality by using the Weather Research and Forecasting Model (WRF) coupled with GEOS-Chem (GC) taking Northwest China as the domain. To properly initialize the model, we studied the effects of using different chemical initial and boundary conditions, different soil maps and the importance of soil moisture spin-up. GC provides better simulated species' concentrations than MOZART-4 by reducing the high bias of ozone, although performances of simulating emitted species such as NO_x are indistinguishable. There is no observable improvement from changing the default soil map to the soil map from Beijing Normal University (BNU) but BNU soil map provides additional value as it is a more recent and higher resolution product. Land surface parameters such as soil moisture are usually neglected in simulation validation. From our spin-up simulations, it is found that soil moisture has not yet attained a stable equilibrium state until two years of simulation. The soil moisture without spin-up also differs from the Global Land Evaporation Amsterdam Model (GLEAM) dataset, which is mostly remote-sensing driven with meteorological reanalysis and thus taking as the

ground truth.

Flooded, sprinkler, drip irrigation schemes are mimicked either by adding water to soil or surface and tuning up transpiration. For the two schemes that directly add water into the land surface model, regional weather and air quality are substantially modified. Sensible heat flux, near surface air temperature and vertical mixing are reduced. The resultant temperature drop due to sprinkler irrigation is about 1°C, and the temperature drop due to flooded irrigation can even reach 2°C. The stability of atmosphere increases by inferring the modified vertical structure over some of the irrigated grid cells. Near surface potential temperature lowers due to cooling, contributing to a stronger near surface gradient of potential temperature but the effects diminish in lower troposphere. The increase in air pollutants is also confined to the near surface region, with a maximum worsening of air quality quantified by the 6 ppb in surface NO_x concentration. On the contrary, ozone does not always increase over the domain but mostly increase around the irrigate cells because of precursors being pushed away from the irrigation centers. By comparing the time series of weather, air quality observations to the simulations, it is found that flooded irrigation reduced the error by about 20%. Although the model fails to capture the actual species concentration, it is merely able to capture the trend and flooded irrigation still gives the best estimates. To conclude, we suggest that drip irrigation is the most preferable option because of its high water saving potential and minimal changes to regional weather and air quality.

Looking ahead, improving site-level air quality simulations deserve great research potential since there is a large room of improvement and high research value to provide more reliable projections for policy makers and farmers. The improved simulation and site-level comparison should give a better projection of the weather

and air quality modification, and decision-making related to irrigation in light of the site-level air quality change.

Appendices

Appendix A. Simulation of the inner domain

Without the nested grid capability in WRF-GC version 1.0, domains are required to run one by one. The inner domain (d02) as shown in Figure A1 is in 3 km × 3 km resolution covering central Gansu, which include two farming sites with observation data. To mimic the nested grid domain supported by WRF but not WRF-GC, the inner domain d02 was simulated using hourly output from d01 for the initial and boundary conditions. All model settings are the same as the larger domain d01 except the resolution as mentioned.

To further improve the model for a better simulation around the farming sites that we have observations, the initial condition of inner domain was slightly modified according to the site observations. The sites are located about 37.8N 102.9E, area of two sites are 400 meters times 200 meters, area of another site is 500 meters times 250 meters. Two sites deploy border irrigation and one site deploys drip irrigation. 2-m air temperature, relative humidity, 10-m wind speed and direction, and surface air pressure were nudged into the input files using WRF Objective Analysis (OBSGRID) utility. OBSGRID physically incorporate the effects of nudging an additional observation by changing also the meteorological field in the vicinity. Several schemes such as Cressman scheme, ellipse scheme, are used in OBSGRID for different purposes including accounting for the deformed wind speed field that affects nudging observations into isobaric levels. However, it should be emphasized that no modification was made to the upper levels because only surface observations are available from the site measurements.

For the comparison between WRF-GC and the observations in the farming sites, preliminary research has been conducted to investigate the difference between WRF-GC using Noah and Noah-MP as two different models, both compared with observations. Without nudging the observations, both LSMs perform quite well in capturing the 2-m temperature at the site. However, the differences of the simulated sensible heat flux and latent heat flux particularly over the site are large (Figure A2). It should be emphasized that these observations are measured in a site where border mulched or drip mulched irrigation is deployed physically, yet in the model there is not any irrigation implemented in these time series figures, and also mulching is not implemented in any simulation.

Observations were also nudged to the initial condition using OBSGRID.

Figure A3 demonstrates the modified initial temperature field due to observation nudged into the inner domain of the model. OBSGRID modifies a circular region of lowered temperature because the temperature at the site is lower than that simulated by WRF-GC in the larger domain. However, since only surface observations are available for nudging, and the site is relatively small compared with the whole domain, the upper tropospheric levels are unaffected and thus the effects of nudging diminishes after a few hours.

To further evaluate the effectiveness of nudging observations, all available WMO stations are being nudged into the model. Only surface data is nudged in order to retain part of the previous practices. Simulation results (Figure A4) find that whenever only surface data is nudged, the model would mostly return to the control simulation without any nudging within a few hours. It is thus suggested to nudge more observations, especially upper air observations into the model such that large scale atmospheric dynamics may be modified.

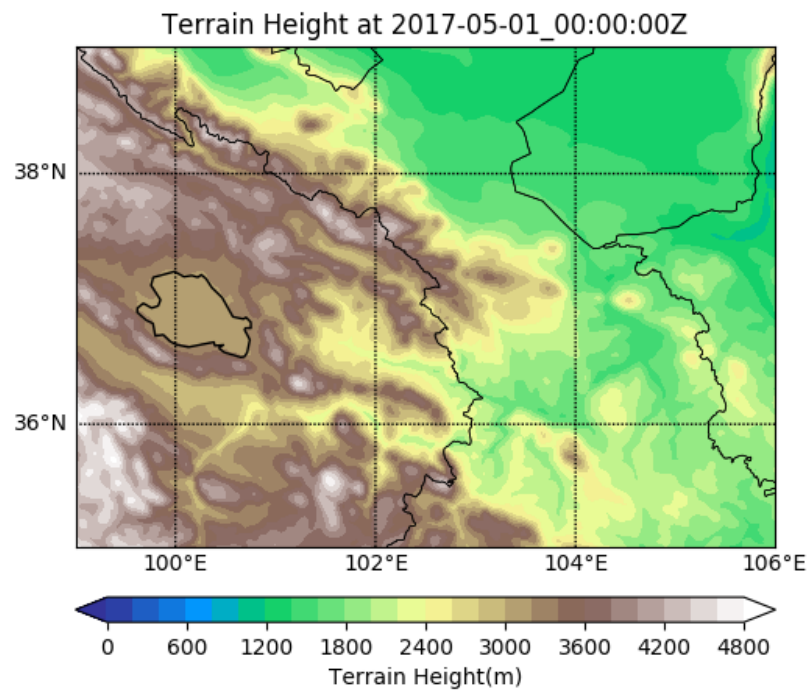
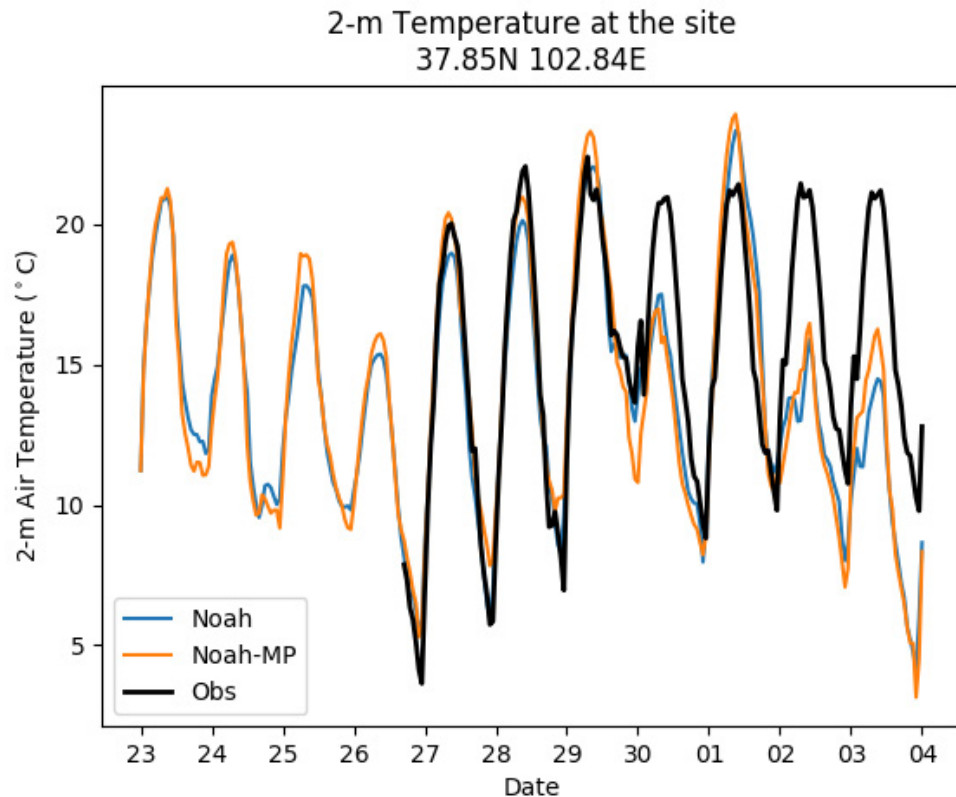
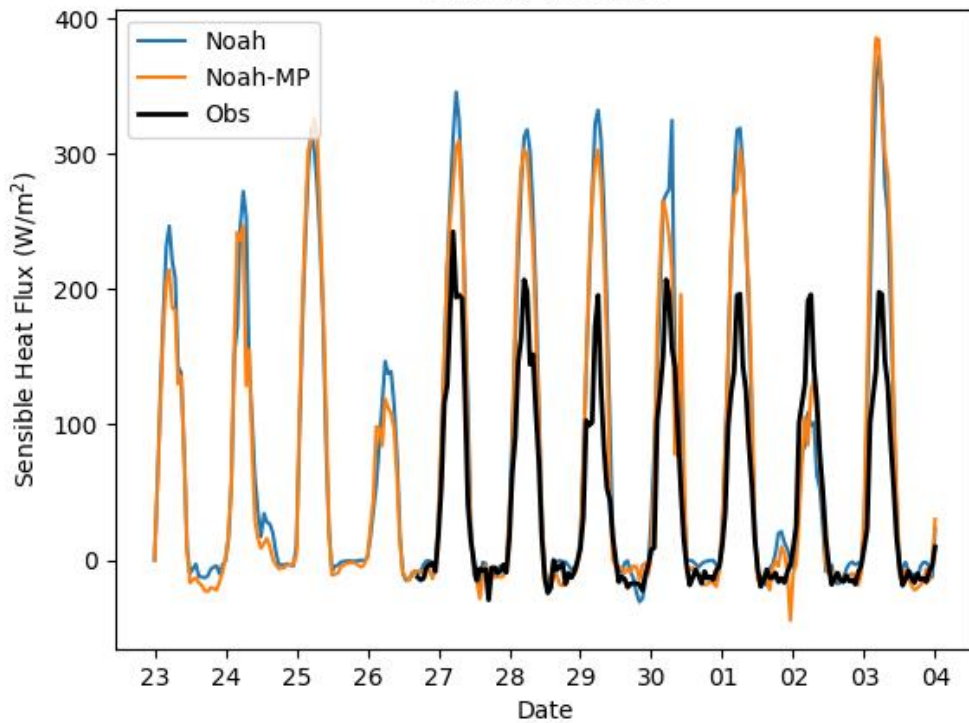


Figure A1. Coverage of the inner domain.



Sensible Heat Flux at the site
37.85N 102.84E



Latent Heat Flux at the site
37.85N 102.84E

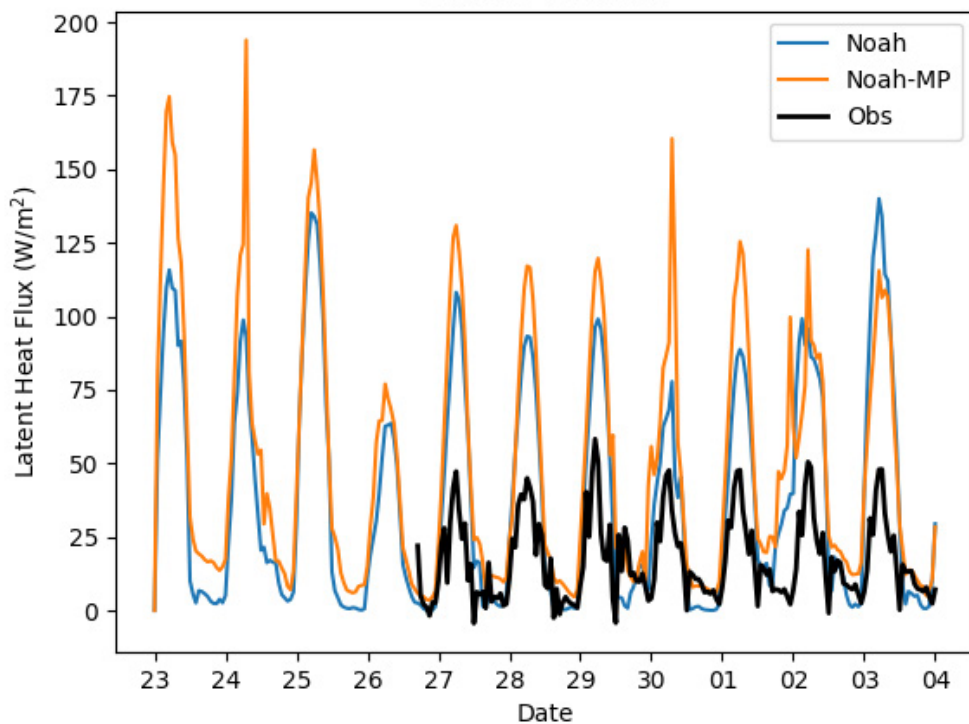


Figure A2. Time series of site observation, and corresponding WRF-GC simulations of (top) 2-m air temperature, (middle) sensible heat flux, (bottom) latent heat flux

using Noah and Noah-MP as the LSMs.

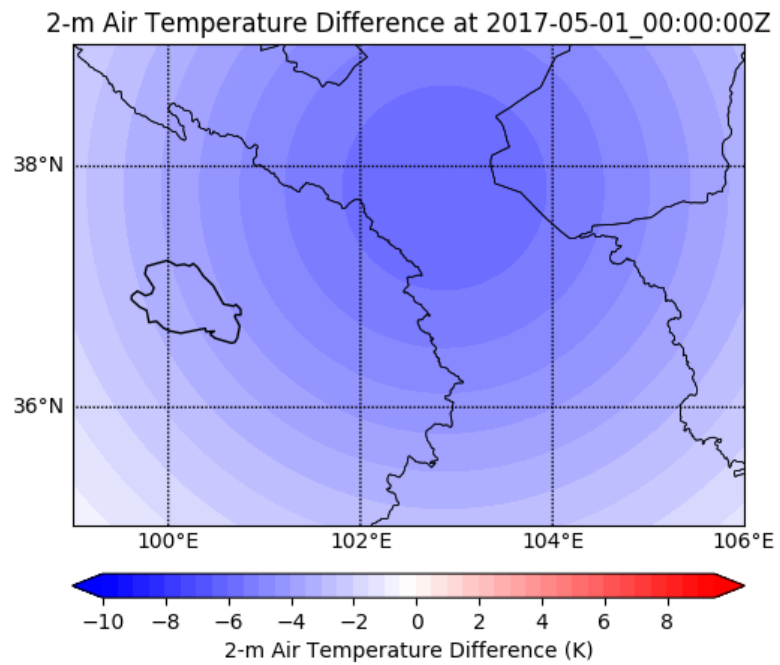


Figure A3. Modified initial temperature field of the inner domain using OBSGRID.

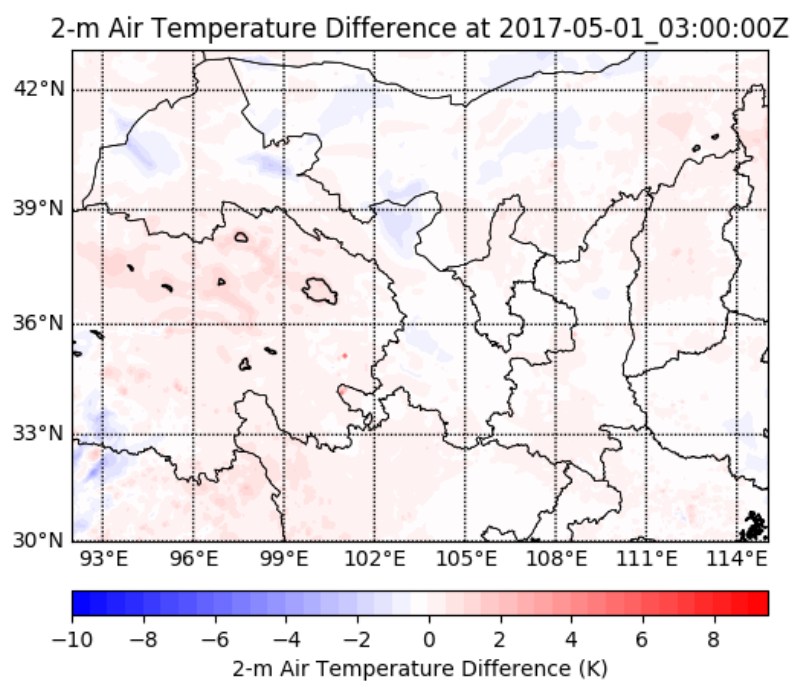
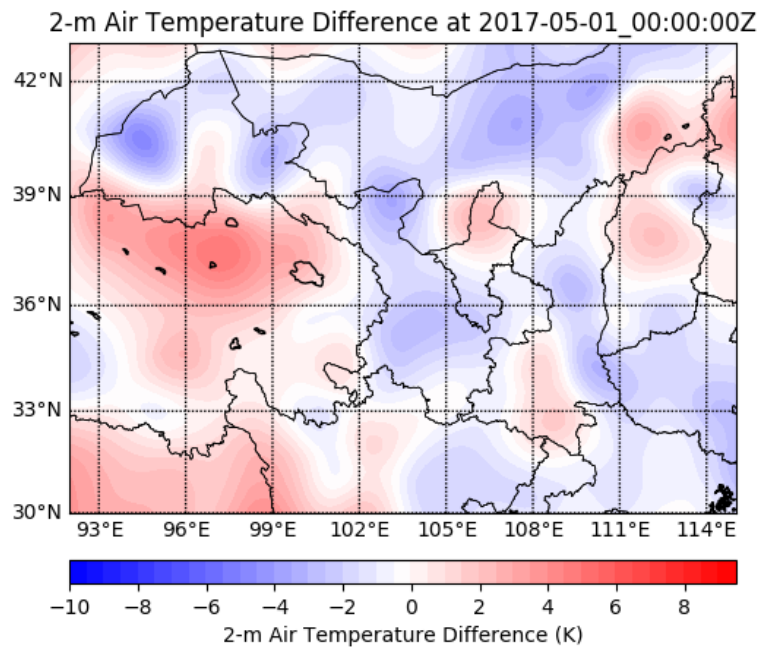


Figure A4. (Top) initial field after nudging all WMO observations; (bottom) temperature difference field after 3 hours of simulation. It can be seen that even with observations nudged, the model is likely to return to its original state after a few hours.

Appendix B. Irrigation parameterization based on realistic irrigation amount

Other than irrigation parameterizations that based on adding soil moisture, precipitation, and transpiration mentioned previously (Evans and Zaitchik (2008); Ozdogan et al. (2010); Lawston et al. (2015)), there are also parameterizations based on realistic irrigation amount (Valmassoi et al., 2020). The irrigation amount is estimated using irrigated area, length of growing season (period of irrigation), and the assumption that irrigation was applied uniformly during the irrigation period. Valmassoi et al. (2020) estimated the irrigation amount of 5.7 mm per day in the Po Valley of Italy. In China, the irrigation water used was 3.32×10^{14} litres in 2016 (China Irrigation and Drainage Development Center, 2016). Total irrigated area was $7.32 \times 10^{11} \text{ m}^2$. In Northwest China for example Gansu province, the dominant crops grown such as maize and soybean are typically grown from May to September, which have a 5-month growing season. Assuming irrigation water is only applied during this 5-month growing season, the irrigation amount over Northwest China is estimated to be 2.96 mm per day. The irrigation water is passed into the model with three irrigation parameterizations that takes three different processes into consideration: (i) the evaporation from the water at soil level; (ii) the canopy interception; and (iii) the drop evaporation and drift. There are three options in the model: option 1 incorporates only process (i); option 2 incorporates processes (i) and (ii); and option 3 incorporates all three processes. Compared with the previous irrigation parameterizations introduced in chapter 2.2, Valmassoi et al. (2020) created a more realistic irrigation simulation in the aspect of actual irrigation water at the expense of irrigation water were assumed to be applied daily, which was usually not the case as shown by field data.

Irrigation parameterizations described in Valmassoi et al. (2020) were implemented in WRF version 4, with debugging in later versions. In this study, WRF version 4.2.2 is used to reproduce the impacts of such irrigation parameterizations to weather over Northwest China domain. The impacts to air quality are not studied because WRF version 4 is not able to couple with GEOS-Chem such that the simulation results cannot be compared with those obtained using WRF-GC that is based on WRF version 3.9.1.1.

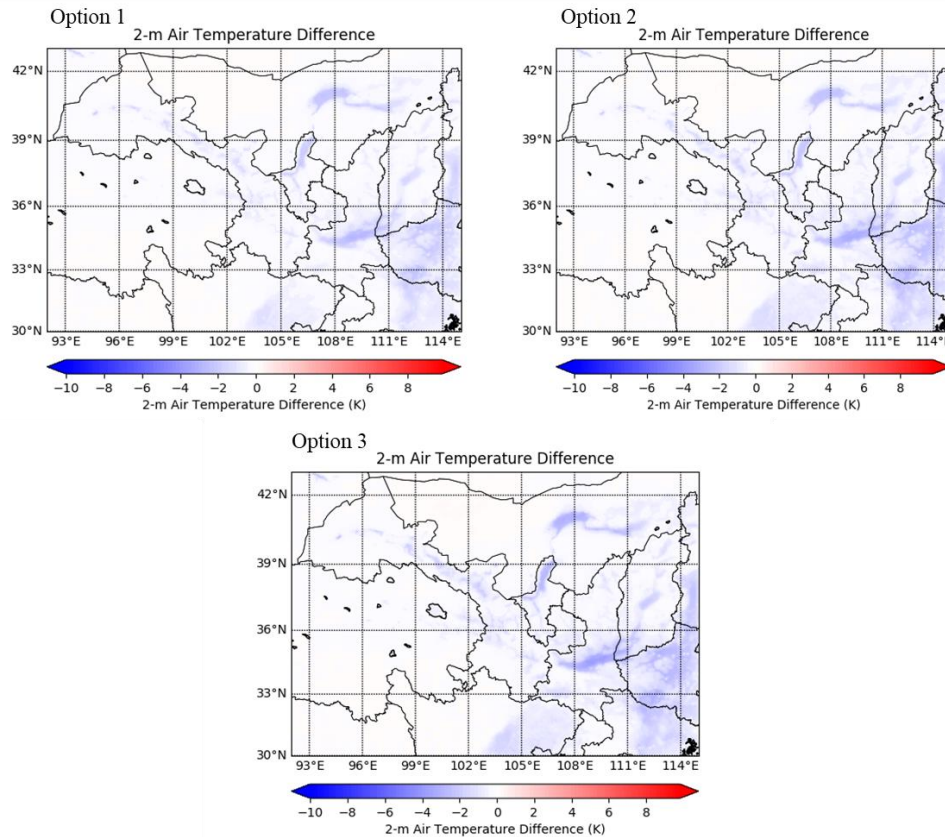


Figure B1. The temperature difference of option 1, option 2, option 3 compared with the control run that does not incorporate any irrigation in the same model.

Figure B1 shows the 2-m air temperature difference of the three irrigation options compared with the control run. Although the simulation results of different options are similar that is in good agreement with Valmassoi et al. (2020), option 3

gives a greatest drop in temperature. It can be attributed to the greatest number of processes being considered in option 3. This irrigation parameterization is not further studied because the parameterization itself is not based on physical intuitions but to modify processes related to water loss that affect evapotranspiration and microphysics processes. More importantly, Valmassoi et al. (2020) demonstrated that the atmosphere and land surface are not highly sensitive to the irrigation timing and duration using the above parameterization schemes that are the weaknesses of other irrigation-related models as field data with relevant information are usually lacking.

Bibliography

- Ambika, A. K., and Mishra, V.: Substantial decline in atmospheric aridity due to irrigation in India, *Environmental Research Letters*, 15(12), 124060, 2020.
- Chen, F., and Dudhia, J.: Coupling an Advanced Land Surface–Hydrology Model with the Penn State–NCAR MM5 Modeling System. Part I: Model Implementation and Sensitivity, *Monthly Weather Review*, 129(4), 569–585, 2001.
- China Irrigation and Drainage Development Center. [2016]. China Irrigation and Drainage Development Research Report. Database accessed on [2021/04/22].
<http://www.jsgg.com.cn/Files/PictureDocument/20180522155908767282130707.pdf>
- Dy, C. Y., and Fung, J. C. H.: Updated global soil map for the Weather Research and Forecasting model and soil moisture initialization for the Noah land surface model, *Journal of Geophysical Research: Atmospheres*, 121, 8777–8800, 2016.
- Emmons, L. K., Walters, S., Hess, P. G., Lamarque, J.-F., Pfister, G. G., Fillmore, D., Granier, C., Guenther, A., Kinnison, D., Laepple, T., Orlando, J., Tie, X., Tyndall, G., Wiedinmyer, C., Baughcum, S. L., and Kloster, S.: Description and evaluation of the Model for Ozone and Related chemical Tracers, version 4 (MOZART-4), *Geoscientific Model Development*, 3, 43–67, 2010.
- Evans, J. P., and Zaitchik, B. F.: Modeling the large-scale water balance impact of different irrigation systems, *Water Resources Research*, 44(8). 2008.
- FAO. [2021]. AQUASTAT Core Database. Food and Agriculture Organization of the United Nations. Database accessed on [2021/02/21].
- Feng, X., Lin, H., Fu, T.-M., Sulprizio, M. P., Zhuang, J., Jacob, D. J., Tian, H., Ma, Y., Zhang, L., Wang, X., and Chen, Q.: WRF-GC (v2.0): online two-way coupling of WRF (v3.9.1.1) and GEOS-Chem (v12.7.2) for modeling regional

atmospheric chemistry-meteorology interactions, Geoscientific Model Development Discuss. [preprint], <https://doi.org/10.5194/gmd-2020-441>, in review, 2021.

Ge, Y., Li, X., Huang, C., and Nan, Z.: A Decision Support System for irrigation water allocation along the middle reaches of the Heihe River Basin, Northwest China, Environmental Modelling & Software, 47, 182-192, 2013.

Gelaro, R., McCarty, W., Suárez, M. J., Todling, R., Molod, A., Takacs, L., Randles, C. A., Darmenov, A., Bosilovich, M. G., Reichle, R., Wargan, K., Coy, L., Cullather, R., Draper, C., Akella, S., Buchard, V., Conaty, A., da Silva, A. M., Gu, W., Kim, G., Koster, R., Lucchesi, R., Merkova, D., Nielsen, J. E., Partyka, G., Pawson, S., Putman, W., Rienecker, M., Schubert, S. D., Sienkiewicz, and M., Zhao, B.: The Modern-Era Retrospective Analysis for Research and Applications, Version 2 (MERRA-2), Journal of Climate, 30(14), 5419-5454, 2017.

Hong, S., Noh, Y., and Dudhia, J.: A new vertical diffusion package with an explicit treatment of entrainment processes, Monthly Weather Review, 134(9), 2318–2341, 2006.

Hou, X. Y., Wang, F. X., Han, J. J., Kang, S. Z., and Feng, S. Y.: Duration of plastic mulch for potato growth under drip irrigation in an arid region of Northwest China, Agricultural and Forest Meteorology, 150(1), 115-121, 2010.

Huber, D. B., Mechem, D. B., and Brunsell, N. A: The effects of Great Plains irrigation on the surface energy balance, regional circulation, and precipitation, Climate, 2(2), 103-128, 2014.

Iacono, M. J., Delamere, J. S., Mlawer, E. J., Shephard, M. W., Clough, S. A., and Collins, W. D.: Radiative forcing by long-lived greenhouse gases: Calculations with the AER radiative transfer models, Journal of Geophysical Research:

Atmospheres, 113, D13103, 2008.

Kang, S., Hao, X., Du, T., Tong, L., Su, X., Lu, H., Li, X., Huo, Z., Li, S., and Ding, R.: Improving agricultural water productivity to ensure food security in China under changing environment: From research to practice, Agricultural Water Management, 179, 5-17, 2017.

Kang, Y., Wang, R., Wan, S., Hu, W., Jiang, S., and Liu, S.: Effects of different water levels on cotton growth and water use through drip irrigation in an arid region with saline ground water of Northwest China, Agricultural Water Management, 109, 117-126, 2012.

Keller, C. A., Long, M. S., Yantosca, R. M., Da Silva, A. M., Pawson, S., and Jacob, D. J.: HEMCO v1.0: a versatile, ESMF-compliant component for calculating emissions in atmospheric models, Geoscientific Model Development, 7, 1409–1417, 2014.

Lawrence, D. M., Fisher, R. A., Koven, C. D., Oleson, K. W., Swenson, S. C., Bonan, G., and Zeng, X.: The Community Land Model version 5: Description of new features, benchmarking, and impact of forcing uncertainty, Journal of Advances in Modeling Earth Systems, 11(12), 4245-4287, 2019.

Lawston, P. M., Santanello, J. A., Zaitchik, B. F., and Rodell, M.: Impact of Irrigation Methods on Land Surface Model Spinup and Initialization of WRF Forecasts, Journal of Hydrometeorology, 16, 1135–1154, 2015.

Li, J., Mahalov, A., and Hyde, P.: Impacts of agricultural irrigation on ozone concentrations in the Central Valley of California and in the contiguous United States based on WRF-Chem simulations, Agricultural and Forest Meteorology, 221, 34-49, 2016.

Li, K., Jacob, D. J., Shen, L., Lu, X., De Smedt, I., and Liao, H.: Increases in surface ozone pollution in China from 2013 to 2019: anthropogenic and meteorological

- influences, Atmospheric Chemistry and Physics, 20(19), 11423-11433, 2020.
- Li, X., Liu, H., Li, J., He, X., Gong, P., Lin, E., Li, K., Li, L., and Binley, A.: Experimental study and multi-objective optimization for drip irrigation of grapes in arid areas of northwest China, Agricultural Water Management, 232, 106039, 2020.
- Lin, H., Feng, X., Fu, T., Tian, H., Ma, Y., Zhang, L., Jacob, D. J., Yantosca, R. M., Sulprizio, M. P., Lundgren, E. W., Zhuang, J., Zhang, Q., Lu, X., Zhang, L., Shen, L., Guo, J., Eastham, S. D., and Keller, C. A.: WRF-GC (v1.0): online coupling of WRF (v3.9.1.1) and GEOS-Chem (v12.2.1) for regional atmospheric chemistry modeling – Part 1: Description of the one-way model, Geoscientific Model Development, 13(7), 3241-3265, 2020.
- Liu, M., Yang, J., Li, X., Liu, G., Yu, M., and Wang, J.: Distribution and dynamics of soil water and salt under different drip irrigation regimes in northwest China, Irrigation Science, 31(4), 675-688, 2013.
- Martens, B., Miralles, D.G., Lievens, H., van der Schalie, R., de Jeu, R.A.M., Fernández-Prieto, D., Beck, H.E., Dorigo, W.A., and Verhoest, N.E.C.: GLEAM v3: satellite-based land evaporation and root-zone soil moisture, Geoscientific Model Development, 10, 1903–1925, 2017.
- Mishra, V., Ambika, A. K., Asoka, A., Aadhar, S., Buzan, J., Kumar, R., & Huber, M. (2020). Moist heat stress extremes in India enhanced by irrigation. Nature Geoscience, 13(11), 722-728.
- Mlawer, E., Taubman, S., Brown, P., Iacono, M., and Clough, S.: Radiative transfer for inhomogeneous atmospheres: RRTM, a validated correlated-k model for the longwave, Journal of Geophysical Research: Atmospheres, 102, 16663–16682, 1997.
- Morrison, H., Thompson, G., and Tatarki, V.: Impact of Cloud Microphysics on the

Development of Trailing Stratiform Precipitation in a Simulated Squall Line:
Comparison of One- and Two-Moment Schemes, Monthly Weather Review,
137, 991–1007, 2009.

Niu, G., Yang, Z., Mitchell, K. E., Chen, F., Ek, M. B., Barlage, M., Kumar, A.,
Manning, K., Niyogi, D., Rosero, E., Tewari, M., and Xia, Y.: The community
Noah land surface model with multiparameterization options (Noah-MP): 1.
Model description and evaluation with local-scale measurements, Journal of
Geophysical Research: Atmospheres, 116, D12109, 2011.

Ozdogan, M., Rodell, M., Beaudoin, H. K., and Toll, D. L.: Simulating the effects
of irrigation over the United States in a land surface model based on satellite-
derived agricultural data, Journal of Hydrometeorology, 11, 171–184, 2010.

Pei, L., Moore, N., Zhong, S., Kendall, A. D., Gao, Z., and Hyndman, D. W.: Effects
of irrigation on summer precipitation over the United States, Journal of
Climate, 29(10), 3541-3558, 2016.

Sacks, W. J., Cook, B. I., Buenning, N., Levis, S., and Helkowski, J. H.: Effects of
global irrigation on the near-surface climate, Climate Dynamics, 33(2), 159-
175, 2009.

Shangguan, W., Dai, Y., Duan, Q., Liu, B., and Yuan, H.: A Global Soil Data Set for
Earth System Modeling, Journal of Advances in Modeling Earth Systems, 6,
249-263, 2014.

Shi, Y., Shen, Y., Kang, E., Li, D., Ding, Y., Zhang, G., and Hu, R.: Recent and
Future Climate Change in Northwest China, Climatic Change, 80, 379–393,
2007.

The International GEOS-Chem Community. (2019, February 28). geoschem/geos-
chem: GEOS-Chem 12.2.1 (Version 12.2.1). Zenodo.

<http://doi.org/10.5281/zenodo.2580198>

Valmassoi, A., Dudhia, J., Di Sabatino, S., and Pilla, F.: Evaluation of three new surface irrigation parameterizations in the WRF-ARW v3.8.1 model: the Po Valley (Italy) case study, *Geoscientific Model Development*, 13, 3179–3201, 2020.

Valmassoi, A., Dudhia, J., Di Sabatino, S., and Pilla, F.: Regional climate impacts of irrigation in northern Italy using a high resolution model, *Atmosphere*, 11(1), 72, 2020.

Wang, L., Tai, A. P. K., Tam, C.-Y., Sadiq, M., Wang, P., and Cheung, K. K. W.: Impacts of future land use and land cover change on mid-21st-century surface ozone air quality: distinguishing between the biogeophysical and biogeochemical effects, *Atmospheric Chemistry and Physics*, 20, 11349–11369, 2020.

Wang, Y., Li, S., Qin, S., Guo, H., Yang, D., and Lam, H. M.: How can drip irrigation save water and reduce evapotranspiration compared to border irrigation in arid regions in northwest China, *Agricultural Water Management*, 239, 106256, 2020.

Wu, L., Qin, F., Feng, J., and Huang, J.: Regional climate effects of plastic film mulch over the cropland of arid and semi-arid regions in Northwest China using a regional climate model, *Theoretical and Applied Climatology*, 139, 335–349, 2020.

Yang, H., Du, T., Qiu, R., Chen, J., Wang, F., Li, Y., Wang, C., Gao, L., and Kang, S.: Improved water use efficiency and fruit quality of greenhouse crops under regulated deficit irrigation in northwest China, *Agricultural Water Management*, 179, 193-204, 2017.

Yang, Z., Qian, Y., Liu, Y., Berg, L. K., Hu, H., Dominguez, F., and Tang, Q.: Irrigation impact on water and energy cycle during dry years over the united

states using convection-permitting WRF and a dynamical recycling model,
Journal of Geophysical Research: Atmospheres, 124(21), 11220-11241, 2019.

Yilmaz, M. T., , Anderson M. C. , , Zaitchik B. , , Hain C. R. , , Crow W. T. , , Ozdogan M. , , Chun J. A. , , and Evans J. , 2014: Comparison of prognostic and diagnostic surface flux modeling approaches over the Nile River basin, Water Resources Research, 50, 386–408, doi:10.1002/2013WR014194.

Zaitchik, B. F., Evans, J., and Smith, R. B.: MODIS-derived boundary conditions for a mesoscale climate model: Application to irrigated agriculture in the Euphrates basin, Monthly Weather Review, 133(6), 1727-1743, 2005.

Zhang, C., and Wang, Y.: Projected Future Changes of Tropical Cyclone Activity over the Western North and South Pacific in a 20-km-Mesh Regional Climate Model. Journal of Climate, 30(15), 5923-5941, 2017.

Zhang, X., Xiong, Z., and Tang Q.: Modeled effects of irrigation on surface climate in the Heihe River Basin, Northwest China, Journal of Geophysical Research: Atmospheres, 122(15), 7881-7895, 2017.

Zhang, Y. L., Wang, F. X., Shock, C. C., Yang, K. J., Kang, S. Z., Qin, J. T., and Li, S. E.: Effects of plastic mulch on the radiative and thermal conditions and potato growth under drip irrigation in arid Northwest China, Soil and Tillage Research, 172, 1-11, 2017.

Zou, H., Fan, J., Zhang, F., Xiang, Y., Wu, L., and Yan, S.: Optimization of drip irrigation and fertilization regimes for high grain yield, crop water productivity and economic benefits of spring maize in Northwest China, Agricultural Water Management, 230, 105986, 2020.